UNIVERSITÀ DI PARMA

DEPARTMENT OF ENGINEERING AND ARCHITECTURE

MASTER OF SCIENCE IN COMMUNICATION ENGINEERING
(LAUREA MAGISTRALE)

INTERPLAY OF MODAL DISPERSION AND NONLINEAR INTERFERENCE IN FIBER OPTIC SYSTEMS

Advisor:
Prof. Paolo Serena

Co-Advisor:

Chiara Lasagni

Master Thesis of:

Reinhardt Rading

ACADEMIC YEAR 2020/2021

Table of Contents

Abstract

Network traffic increases by 30% percent each year and is even expected to increase by a greater margin as more people and devices are getting connected to the internet. During this COVID-19 period, optical networking vendors have reported experiencing an unpredictable surge in data demands that are stressing the existing optical networks. Studies have shown that we are almost approaching the capacity crunch of single-mode fibers, and since the current optical networks are mainly made of single-mode fibers, we need new technologies to meet these increasing demands. Space division multiplexing, elastic optical networks, high order modulation formats are some of the technologies being proposed with each technology having its pros and cons. Space division multiplexing (SDM) has received a lot of attention as an alternative solution and it involves exploiting the spatial diversity of optical fibers in the form of polarization, the number of modes, number of cores or fibers working as bundles. Although SDM fibers represents a promising solution compared to the current single-mode fibers, such fibers introduce new challenges due to the interactions among the propagating modes.

In ideal optical fibers, birefringence does not exist, and thus optical modes propagate inside the fiber without coupling. In practical cases, birefringence manifests itself due to imperfections, such as imperfect circular symmetry during the fiber manufacture, or due to external stresses, such as mechanical pressure exerted after manufacturing. This asymmetry results in random perturbation causing the two field polarizations to have different group delays, hence polarization mode dispersion (PMD) arises. In a multi-mode fiber, random birefringence leads to spatial mode dispersion (MD) among the different spatial models, in addition to the PMD among the polarizations of each mode.

This thesis investigated the impact of PMD and SMD on optical fiber transmissions, especially focusing on its interaction with the nonlinear interference (NLI) arising during the signal propagation along the optical fiber. With this aim, we exploited the Gaussian noise (GN) model extended to include PMD and SMD to estimate the cross-channel nonlinear interaction. Such a closed-form expression allows to quickly estimate the impact of SMD on non-linearities for several transmissions and links configurations. We also performed numerical simulations by means of the Split Step Fourier method (SSFM) to confirm the model prediction. The obtained results showed that modal dispersion can be very beneficial in reducing the NLI in various scenarios. In particular, we tested different

optical systems in terms of: dispersion, attenuation, channel spacing, symbol rate, and number of modes.

Introduction

The invention of lasers [1] and the discovery that impurities in the glass medium caused hundreds of losses in decibels [2] in 1960s spurred a greater development in optical fiber communications. Later in the 1980s after intensive research and development in photonic devices, optical fiber replaced coaxial cable systems as a means of transmitting information because of its low cost and attenuation, lighter and immunity to electromagnetic interference. The development of erbium doped fiber amplifier, wavelength division multiplexing, elastic and mixed rate optical networks, allowed higher achievable transmission rates to grow exponentially; with a compound annual growth rate of tenfold every four years.

These developments in optical fiber communications has seen more people being connected to the internet and was seen as a luxurious opportunity by the vendors as the demands keep growing every year [3]. Network demand continues to grow at more than 30% per year and is even expected to grow further with the introduction of technologies like cloud computing and internet of things where more devices are being connected to the internet. According to Orange Telecom, the predicted 30 % yearly increase in demands is way below the real demands and that we should expect a more and more demands in the coming years. In this COVID-19 period, we are witnessing unpredictable increase in data demands that are stressing the existing optical fiber networks [4]. Furthermore, Cisco predicts that an average 19% compound annual growth in internet users in 2022 and a global internet protocol traffic reaching an all time high annual rate of 4.8 zettabytes by the end of the year [5].

Most optical networks currently are made up of single mode fibers (SMF). Such fibers currently provide an infrastructure for transmitting ultra high capacities. However, studies have shown that there is a capacity limit [6] resulting from the non-linear response of fiber optic systems and that such a limit is likely to reached soon yielding a capacity crunch [7]. Claude Shannon in [8] showed that the capacity of a channel with additive white Gaussian noise can be calculated as,

$$C = Blog_2(1 + SNR) \tag{1}$$

where C is the capacity, B is the bandwidth, SNR is the signal to noise ratio -referred to as OSNR in optical communications,i.e., is the ratio of the signal power to noise power, mainly caused by amplified spontaneous emission. From equation 1, the channel capacity

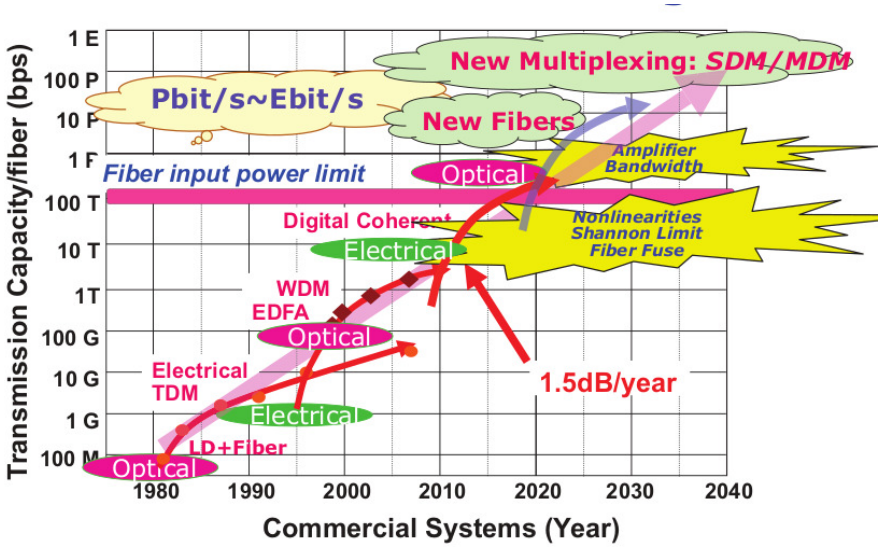

Figure 1: Evolution of optical fiber transmission technologies [9].

explicitly depends on the bandwidth and the OSNR. One might argue that to increase the capacity, one could increase the SNR by increasing the power of the signal. While this is true in a channel with additive white Gaussian noise, the same is untrue for a fiber optic channel which has a multiplicative noise and a non-linear response to an increase in power and distance. The input-output relationship of an optical fiber channel involves solving a partial differential equation that does not have a closed form solution. Hence, a keen analysis is required to explore ways to combat non-linearity.

The approaching capacity crunch in single mode fibers has galvanized researchers to find ways to navigate this capacity crunch challenge. Several technologies have been proposed including, but not limited to, spatial division multiplexing (SDM), ultra-wide band (UWB) fiber optic systems, elastic optical networks, high order modulation formats. Each solution seems to have its own advantages and disadvantages, and a preference from different researchers.

Multi-band optical fiber systems involve using all the wavelengths between 1280nm to 1700nm. Researchers in [10] claim that this technology is advantageous as it shifts the current channel bandwidth from between 5-11.5 terahertz (C- and C+L band) to 53.5 terahertz (O, E, S, C, L bands) and that the multi-band system will use the already existing fiber infrastructure. The main drawback is the requirement of new amplification devices for the multi-band system.

Space division multiplexing has received a lot of attention lately and it entails manipulating the spacial diversity in optical fibers in form of fiber bundles, multicore (MMF) or multimode fibers(MCF). Unlike in SMF where the core diameter is between 5 to 12 micrometers and only one mode propagates, in SDM several modes propagate thus opening a real channel parallelization that is known to be the best solution to increase the

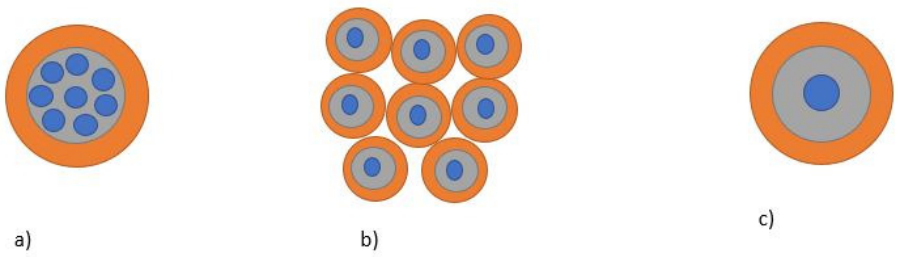

Figure 2: Space division multiplexed system with a)Multi-core fiber, b) Fiber bundles, c) Multi-mode fiber

capacity.

The drawback of this technology according to [10] is that it would mean a complete fiber infrastructure replacement, the technology is not mature, and a complex digital signal processing at the receiver.

The Shannon channel capacity in optical fibers as shown in equation 1 changes to

$$C = 2 \times B \times M \times log_2(1 + GSNR) \tag{2}$$

according to [11] when the above proposed technologies are implemented. B is the optical bandwidth, M is the number of spacial optical paths that can be manipulated and GSNR is the generalized signal to noise ratio given by

$$GSNR = \frac{P_s}{P_{ASE} + P_{NLI}} \tag{3}$$

where P_{ASE} is the power of amplified spontaneous emission and P_{NLI} is the power of the non-linear impairments and P_s is the power of the signal transmitted in the fiber. Just like in SMF fibers that experiences both linear and non-linear effects, the same effects are experienced in SDM systems but with a different degree with some linear effects having been proved to be beneficial in combating non-linearities during the signal propagation [12]. Mode coupling and mode dispersion are the main linear effects that studies have shown to be beneficial in combating non-linearities. Strong mode coupling is also beneficial in reducing the delay spread factor between the modes and thus a reduced complexity at the receiver. Studies had further shown that a huge mode dispersion tends to reduce the non-linear Kerr effects and thus an improved system performance when it is allowed on the link.

In this thesis, i will focus on the interplay between mode dispersion and non-linear interference in fiber optic systems. I will show that a strong mode dispersion is in-fact beneficial in combating cross-phase modulation and other non-linearities. Furthermore, I

will shown that by increasing mode dispersion and varying other system parameters for example dispersion, symbol rate, attenuation,span length, the quality of transmission in fiber optic systems is improved. The analysis is done both by means of split step Fourier simulations and by using an ultrafast analytical Gaussian noise model, which is able to capture the average or ergodic behaviour of non-linear variance.

The thesis is structured as follows, the first chapter discusses the linear propagation in optical fibers, discussing the propagation in the scalar case and extending to the multimode case. Attenuation, coupling, and mode dispersion are discussed. At the end of the chapter, the thesis discusses the two linear propagation model-power and matrix model.

The second chapter outlines the non-linear propagation in both the scalar and mode division multiplexed systems. In this chapter we derive the non-linear Schroedinger equation for MDM systems. The chapter further analyses the non-linear impairments in terms of both intra and inter group interference and how mode dispersion reduces these impairments.

Chapter three discusses the work done and the results obtained. It shows how the quality of transmission is improved when mode dispersion is enhanced. In this chapter, I compare the results obtained from the GN model extended for mode dispersion with the results from the SSFM simulations. The final chapter concludes the thesis and describes the possibility of future work.

Chapter 1

Linear Propagation in Optical Fiber Systems

This chapter introduces linear propagation in optical fibers. The first part describes linear propagation in single mode fibers while the second part focuses on the multimode scenarios.

1.1 Linear propagation in scalar case

In absence of nonlinear effects and birefringence, the propagation of the electric field in a single mode fiber can be described through the linear Schrödinger [14] equation as shown:

$$\frac{dE}{dZ} = -\frac{\alpha}{2}A - \beta_1\frac{dE}{dt} + j\frac{\beta_2}{2}\frac{d^2E}{dt^2} + \frac{\beta_3}{6}\frac{d^3E}{dt^3} \tag{1.1}$$

where α is the attenuation constant, β_1 is the group delay, β_2 is the group velocity dispersion and β_3 is the third order dispersion.

We now discuss the impact of each effect separately.

1.1.1 Attenuation

Signal attenuation in an optical fiber is caused by material absorption and scattering (linear and nonlinear scattering), micro and macro bending, mode coupling losses and losses resulting from splitters and connectors. The change in power from the input to the output is governed by Beer's law given by:

$$\frac{dP}{dz} = -\alpha P. \tag{1.2}$$

Consider a fiber of length L. If P_{in} is the input power, the output power P_{out} is related to the input power by:

$$P_{out} = P_{in} \exp(-\alpha L). \tag{1.3}$$

The attenuation constant is usually measured in $\frac{dB}{km}$ and is calculated as:

$$\alpha \left[\frac{dB}{km}\right] = \frac{-10}{L} \log_{10}\left(\frac{P_{out}}{P_{in}}\right) \equiv 4.343\alpha. \tag{1.4}$$

1.1.2 Group delay

A bandpass signal like an electric field, propagates inside the fiber with a group velocity, which can be related to the frequency and the propagation constant β by:

$$V_g = \left.\frac{d\omega}{d\beta}\right|_{\omega_0} \tag{1.5}$$

where ω_0 is the carrier angular frequency. The group delay is given as the inverse of group velocity. The group delay in (1.1) is given by:

$$\beta_1 = \frac{1}{V_g}. \tag{1.6}$$

1.1.3 Group velocity dispersion (GVD)

Fiber dispersion is the linear process at which a pulse sent in a dielectric material like an optical fiber broadens. It is caused by the material, waveguide or intermodal dispersion. Both material and waveguide dispersions are categorised as chromatic dispersion and are experienced in both single and multimode fibers whereas only intermodal dispersion is experienced in multimode fibers. This broadening of the pulse causes inter-symbol interference at the receiver since the receiver is unable to distinguish between the pulses as it overlaps with other pulses.

For instance, in a single mode fiber of length L, a signal at frequency ω in the absence of GVD, will arrive at the end of the fiber with a time delay T given by:

$$T = \frac{L}{V_g}. \tag{1.7}$$

The frequency dependence on the group velocity means that pulses of different frequencies will arrive at the receiver at different times. If $\Delta\omega$ is the spectral width of the pulse, the pulse broadening experienced on a fiber of length L is given by:

$$\Delta T = \frac{dT}{d\omega}\Delta\omega = \frac{d}{d\omega}\left(\frac{L}{V_g}\right)\Delta\omega = L\frac{d^2\beta}{d\omega^2}\Delta\omega \tag{1.8}$$

where is $\frac{d^2\beta}{d\omega^2}$ is the GVD parameter, β_2 in (1.1). By using

$$\omega = \frac{2\pi c}{\lambda} \tag{1.9}$$

and

$$\Delta\omega = -\frac{2\pi c}{\lambda^2}\Delta\lambda, \tag{1.10}$$

(1.8) can be written as:

$$\Delta T = \frac{d}{d\lambda}\left(\frac{L}{V_g}\right)\Delta\lambda = DL\Delta\lambda \tag{1.11}$$

where D is the dispersion parameter given by:

$$D = \frac{d}{d\lambda}\left(\frac{1}{V_g}\right) = -\frac{2\pi c}{\lambda^2}\beta_2. \tag{1.12}$$

If we consider only group velocity dispersion, the linear propagation equation in (1.1) changes to:

$$\frac{dE}{dz} = j\frac{\beta_2}{2}\frac{d^2E}{dt^2} \tag{1.13}$$

which can further be rewritten as:

$$\frac{dE}{dz} = \frac{j}{2}\text{sign}(\beta_2)\frac{\tau_0^2}{\tau_0^2}\frac{d^2E}{dt^2} \tag{1.14}$$

where τ is the normalized time and the the ratio of τ_0^2 to $|\beta_2|$ is the dispersion length L_D. A pulse of frequency transform $A(0,\omega)$ will experience GVD such that after distance z, the pulse takes the expression:

$$A(z,\omega) = e^{-j\frac{\beta_2}{2}\omega^2 z}A(0,\omega). \tag{1.15}$$

GVD is a unitary operation: although there is pulse distortion, energy is saved:

$$\int_{-\infty}^{\infty}|A(z,t)|^2dt = \int_{-\infty}^{\infty}|A(z,\omega)|^2\frac{d\omega}{2\pi} = \int_{-\infty}^{\infty}|A(0,\omega)|^2|e^{-j\frac{\beta_2}{2}\omega^2 z}|^2\frac{d\omega}{2\pi}. \tag{1.16}$$

The square of the exponential including the GVD parameter on the third term of (1.16) is equivalent to one and thus when reconverted to time domain we get the initial pulse with no energy changes. GVD also doesn't alter the symmetry of the pulse implying that the pulse symmetry is the same prior and after GVD.

$$A(z,\omega) = A(0,\omega)e^{-j\frac{\beta_2}{2}\omega^2 z} \equiv A(0,-\omega)e^{-j\frac{\beta_2}{2}(-\omega)^2 z} \equiv A(z,-\omega). \tag{1.17}$$

If a pulse is transmitted in a high dispersive optical fiber such that GVD value is very large, the pulse at the output of the fiber is the Fourier transform of the pulse at the

input. For example, if we transmit a rectangular pulse in a high dispersive fiber, we will get a sinc shaped pulse amplitude at the output due to GVD.

The problem of pulse broadening can be counteracted by designing a fiber with zero dispersion, i.e by using dispersion shifted fiber. Alternatively, GVD can be eliminated by inserting dispersion compensating fiber (DCF) which usually has a smaller effective area compared to the transmission fiber. Another solution is based on using electronic dispersion compensation, coding or adding a chirp to the laser.

There exists two types of dispersion management in optical links; dispersion uncompensated and dispersion managed links. The difference between the two is that in dispersion uncompensated links there is no recovery of dispersion within the link, it is recovered in a lumped way at the receiver or transmitter. In dispersion managed links-the accumulated GVD is indeed regularly recovered during the signal propagation by means of dispersion compensating fibers, that leaves a small residual dispersion value is left on the link. Several studies have shown the supremacy of dispersion uncompensated links in mitigating the accumulation of the nonlinear interference due to the Kerr effect along the link.

At large bandwidth it is also important to include the variation of β_2 along frequency, which is accounted by the β_3 parameter, usually called third order dispersion.

1.1.4 Polarization mode dispersion

Equation (1.1) is for scalar propagation. In the presence of polarization effects, the electric field can be described by a vector

$$\vec{E}(z,t) = \begin{bmatrix} E_x(z,t) \\ E_y(z,t) \end{bmatrix} \tag{1.18}$$

such that

$$\vec{E} = \left(\hat{x} E_x e^{j\phi_x} + \hat{y} E_y e^{j\phi_y} \right) e^{j(\omega_0 t - \beta z)} \tag{1.19}$$

where $\hat{x}$ and $\hat{y}$ are the unit vectors in x and y directions, $E_x(z,t)$ is the electric field in the x-polarization and $E_y(z,t)$ is field on the y-polarization; ϕ_x and ϕ_y are the phases of the x and the y component respectively; ω_0 is the angular carrier frequency and β is the propagation constant.

In an ideal SMF fiber, the group velocity of the two orthogonal polarizations is the same, but in practical cases there exists birefringence arising from the imperfections during the fiber manufacture or arising from mechanical pressure exerted after manufacturing. These asymmetries result in non-degeneracy of the group delays of the two polarization tributaries, that thus experience different group delays hence polarization mode dispersion. Birefringence can be defined by

$$\Delta\beta = \frac{\beta_x - \beta_y}{\frac{2\pi}{\lambda}} \tag{1.20}$$

where β_x is the propagation constant of the electric field on the x-direction and β_y is the propagation constant in the y-direction. We thus a differential speed given by

$$V_g = \frac{1}{\frac{d(\Delta\beta)}{d\omega}}. \tag{1.21}$$

We can generalize (1.1) to include PMD as:

$$\frac{d\vec{A}}{dZ} = j\beta(\omega)\vec{A} \tag{1.22}$$

where

$$\vec{A}(z,\omega) = \tilde{T}(\omega)\tilde{A}(0,\omega) \tag{1.23}$$

represents the input-output propagation equation. $\vec{A}(z,\omega)$ is the Fourier transform of $\vec{A}(z,t)$ given by

$$\vec{A}(z,\omega) = \int_{\infty}^{\infty} \vec{A}(z,t)e^{-j\omega t}dt \tag{1.24}$$

where

$$\vec{A}(z,t) = E(z,t)\left(\frac{A_{eff}}{2Z_0}\right)^{\frac{1}{2}} \tag{1.25}$$

and

$$\tilde{T}(\omega) = exp\left[-\frac{\alpha}{2} - j\beta_1\omega - j\frac{\beta_2}{2}\omega^2\right]z. \tag{1.26}$$

Considering the two degree of freedoms resulting from the two polarizations, (1.22) and (1.23) changes to

$$\frac{d\vec{A}}{dZ} = j\mathbf{B}(\omega)\tilde{\mathbf{A}} \tag{1.27}$$

$$\vec{A}(z,\omega) = \mathbf{T}(\omega)\tilde{A}(0,\omega) \tag{1.28}$$

with $\mathbf{B}$ a Hermitian matrix and $\mathbf{T}$ a unitary matrix. In the polarization maintaining fiber, the propagation can be modelled as

$$\frac{d\vec{A}}{dZ} = j\mathbf{B}(\omega)\tilde{\mathbf{A}} = -\mathbf{jL}\begin{Bmatrix}\beta_x & 0\\ 0 & \beta_x\end{Bmatrix}\mathbf{L}^{\dagger}\tilde{\mathbf{A}}(\omega) \tag{1.29}$$

with $\mathbf{L}$ a random 2X2, unitary Haar matrix.

A real fiber can be described as a concatenation of polarization maintaining fibers according to the wave plate model. According to [15], [16], we subdivide the fiber, into a concatenation of statistically independent sections as depicted in fig. 1.1.

$$\mathbf{L}\begin{bmatrix}e^{j\beta_x^{(1)}\Delta z} & 0\\ 0 & e^{j\beta_y^{(1)}\Delta z}\end{bmatrix}\mathbf{L}^{\dagger}. \tag{1.30}$$

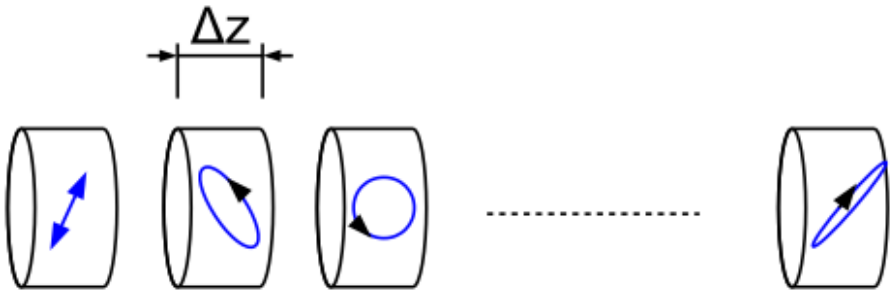

Figure 1.1: Subdivides the fiber of length L into a concatenation of statistically independent polarization maintaining fibers

Each section of the divided fiber is described by the coupling matrix in (1.30) and the overall fiber is described by the concatenation of all the sections, i.e:

$$\mathbf{L_1}\begin{bmatrix} e^{j\beta_x^{(1)}\Delta z} & 0 \\ 0 & e^{j\beta_y^{(1)}\Delta z} \end{bmatrix}\mathbf{L_1}^{\dagger}\mathbf{L_2}\begin{bmatrix} e^{j\beta_x^{(2)}\Delta z} & 0 \\ 0 & e^{j\beta_y^{(2)}\Delta z} \end{bmatrix}\mathbf{L_2}^{\dagger}\mathbf{L_3}\begin{bmatrix} e^{j\beta_x^{(3)}\Delta z} & 0 \\ 0 & e^{j\beta_y^{(3)}\Delta z} \end{bmatrix}\mathbf{L_3}^{\dagger}\cdots\mathbf{L_N}\begin{bmatrix} e^{j\beta_x^{(N)}\Delta z} & 0 \\ 0 & e^{j\beta_y^{(N)}\Delta z} \end{bmatrix}\mathbf{L_N}^{\dagger} \tag{1.31}$$

where Δz is the correlation length which is the length where the birefringence changes.

1.2 Linear propagation in mode multiplexed systems

Consider a fiber that supports N modes during propagation with the total number of scalar modes being 2N considering the degree of freedom provided by the two polarization. The electric field propagating along the fiber can then be written as:

$$\vec{E}(r,t) = Re\left[\sum_{n=1}^{2N} \frac{\vec{F}_n(x,y,\omega_0)}{N_n(\omega_0)} E_n(z,t)e^{-i\omega_0 t}\right] \tag{1.32}$$

$E_n(z,t)$ is the complex field of the n-th mode and it evolves during propagation. $N_n(\omega_0)$ is the coefficient used to normalize and ensure that the power (in watts) carried in each mode is equivalent to $|E_n(z,t)|^2$ while $\vec{F}_n(x,y,\omega_0)$ is the lateral profile of the nth mode and is orthogonal to each other lateral profile. Both the lateral profile and the normalization coefficient are independent of distance. Defining $|E_n(z,t)\rangle$ as a hyper-polarization vector - a column vector with 2N complex envelopes, it's Fourier transform is given by:

$$|E(z,\omega)\rangle \quad = \sum_{n=1}^{2N} \int E_n(z,t)e^{-i\beta\omega t}dt. \tag{1.33}$$

In the absence of non-linearity, the linear propagation of the complex envelope is described by:

$$\frac{d|\tilde{E}\rangle}{dz} = i\mathbf{B}|\tilde{E}\rangle \tag{1.34}$$

where $\mathbf{B}(z,\omega)$ is a $2N \times 2N$ Hermitian matrix describing the evolution of the hyper-polarization vector during propagation. Vector $\mathbf{B}(z,\omega)$ can be expanded by using the Taylor series and rewritten as

$$\mathbf{B}(z,\omega) = \mathbf{B}^{(0)} + \mathbf{B}^{(1)}\omega + \frac{\mathbf{B}^{(2)}\omega^2}{2}. \tag{1.35}$$

In an ideal fiber structure where there is no mode coupling, matrix $\mathbf{B}(z,\omega)$ is diagonal [16]. In real cases it is never diagonal due to imperfections during fiber manufacturing. The components of the vector $\mathbf{B}(z,\omega)$ includes $\mathbf{B}^{(0)}$ that describes the propagation constant of each mode β_n, $\mathbf{B}^{(1)}$ that describes the inverse group velocity of each mode and $\mathbf{B}^{(2)}$ that describes the group velocity dispersion of each mode. The effect of fiber imperfection highly affects the propagation constants $\mathbf{B}^{(0)}$ and has little effect on the inverse group $\mathbf{B}^{(1)}$ and little to no-effect on the group velocity dispersion $\mathbf{B}^{(2)}$. As a result of such imperfections, the state of hyper-polarization rotates randomly during propagation.

We assume that the N modes supported by the fiber can be grouped into quasi-degenerate groups meaning that modes with similar $\Delta\beta$ are grouped together. For example, we assume that a fiber supports 2 groups of N_a and N_b modes such that the number of scalar modes in each group is $2N_a$ and $2N_b$ respectively. See fig. 1.2 for an example.

The linear propagation equation in group a in the above case becomes:

$$\frac{d|E_a\rangle}{dz} = j\mathbf{B}_a^{(0)}|E\rangle - \mathbf{B}_a^{(1)}\frac{d|E_a\rangle}{dt} - j\frac{\beta_a''}{2}\frac{d^2|E_a\rangle}{dt^2} + j\mathbf{K}_{ab}|E_b\rangle \tag{1.36}$$

and the propagation equation in group b becomes:

$$\frac{d|E_b\rangle}{dz} = j\mathbf{B}_b^{(0)}|E\rangle - \mathbf{B}_b^{(1)}\frac{d|E_a\rangle}{dt} - j\frac{\beta_b''}{2}\frac{d^2|E_b\rangle}{dt^2} + j\mathbf{K}_{ab}^{\dagger}|E_a\rangle \tag{1.37}$$

where β_a'' and β_b'' are the mode-average chromatic dispersion coefficient of the two mode groups and $\mathbf{K}_{ab}(z)$ is a $2N_a \times 2N_b$ matrix accounting for the random linear coupling between the two groups.

1.3 Mode coupling

The fiber imperfections discussed in the previous section cause a perturbation in the fiber resulting in mode coupling. As a consequence, the propagating fields to evolve randomly. Several studies have shown that a reduction in digital signal processing complexity at the receiver can be gained if the coupling is restricted to occur within the mode groups [17], [25]. It has also been shown in [18] that mode coupling can be beneficial in reducing the group delay spread in mode multiplexing systems and that strong mode coupling could

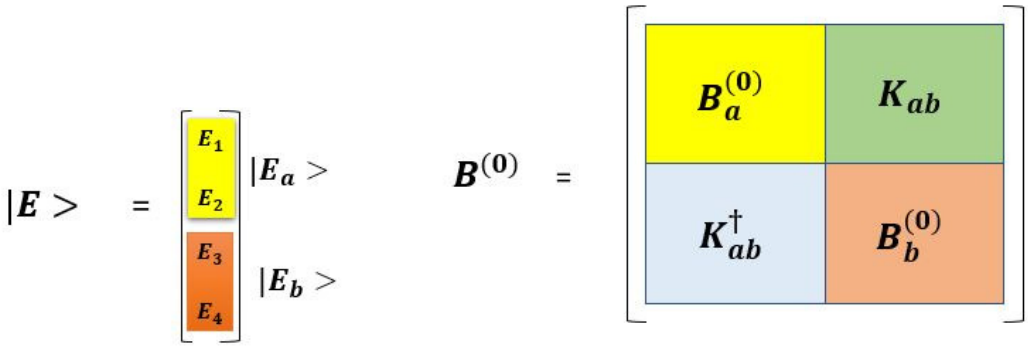

Figure 1.2: Complex envelopes E_1 and E_2 belong to the same group a, while E_3 and E_4 belong to group b. $\mathbf{K}_{ab}(z)$ is a $2N_a \times 2N_b$ matrix accounting for the random linear coupling between the two groups.

also beneficial in reducing mode dependent loss inducing power variations and channel capacity fluctuations between the modes [19].

Mode coupling can be categorised into either strong mode coupling or weak mode coupling. Strong coupling occurs among modes having nearly equal propagation constants while weak coupling occurs among modes having unequal propagation constant especially with large propagation constant difference. Modes with almost equal propagation constant couple over a distance between ten to a hundreds of meters [20], whereas the coupling between modes with a huge propagation constant difference occurs after several kilometres of propagation [21].

Coupling between modes can be described by two models: a field coupling model or a power coupling model. The field coupling model describes the complex field coupling and thus can explain the changes experienced in the eigenmodes and eigenvalues during propagation. The power coupling model describes the power sharing between the modes but is not able to model the changes experienced by the eigenmodes and eigenvalues of the modes.

1.3.1 Field coupling model

As shown in [12], we assume that light travels along the z-direction and we define (x, y) as a transverse plane and $n_0(x, y)$ as the unperturbed refractive index. This refractive index is independent of the z coordinate. Solving the wave equation that is dependent on $n_0^2(x, y)$, we get M orthonormal ideal propagating fields. Let $E(x, y)$ denote one of the modal fields thus for M fields

$$E_u(x,y) \qquad u = 1, 2, 3, \cdots, M \tag{1.38}$$

having a propagation constant β_u where $u = 1, 2, 3, \cdots, M$. The complete electric field can be written as

$$E(x,y,z) = \sum_{u=1}^{M} A_u(z) E_u(x,y). \tag{1.39}$$

If the fiber index profile is perturbed along the spatial coordinates then the electric fields describing different modes couple together yielding

$$\frac{A_u}{dz} = -j\beta_u A_u + \sum_{v \neq u} C_{uv}(z) A_v \quad u = 1, \cdots, M \tag{1.40}$$

where the first term on the right hand side of (1.40) describes the uncoupled propagation while the second term describes coupling between modes with $C_{uv}(z)$ the coupling coefficient. The propagating field can also be written as a reference system tracking the propagation constants.

$$E(x,y) = \sum_{u} A_u(z) E_u(x,y) e^{-j\beta_u z}. \tag{1.41}$$

To understand the implications of this model, assume at z=0 only one mode v is excited and that all the other modes having $u \neq v$ are weakly coupled during propagation.

$$A_v(0) = 1 \quad A_u(0) = 0 \quad |A_v(z)| << |A_u(z)| \tag{1.42}$$

After distance L, the field of mode u is given by

$$A_u(L) = e^{-j\beta_u L} \int_0^L C_{uv}(z) e^{-j(\beta_v - \beta_u)z} dz \quad u \neq v. \tag{1.43}$$

The integral on the right hand side of (1.43) defines the phase matching condition and how coupling depends on the propagation constant.

1.3.2 Power coupling model

The power coupling model describes the distribution of power between modes [13]. The power for any given mode is denoted by

$$P_u(z) = \langle |A_u(z)| A_u(z) \rangle \tag{1.44}$$

and their evolution is given by

$$\frac{dP_u}{dz} = \alpha_u P_u + \sum_{v \neq u} h_{uv}(P_u - P_v), \qquad u = 1, \cdots, M \tag{1.45}$$

where $\alpha_u P_u$ is the loss by power attenuation while the second term on the right hand side of (1.45) is the coupling between modes. Just like in the field model, the coupling coefficient in the power model is given by

$$h_{uv} = \left\langle \left| \int_0^L C_{uv}(z) e^{-j(\beta_v - \beta_u)z} \; dz \right|^2 \right\rangle. \tag{1.46}$$

To understand the model better, assume a case of two modes, the coupling equations become:

$$\frac{dP_a}{dz} = \alpha P_a h_{ab}(P_b - P_a) \qquad \text{mode a} \tag{1.47}$$

$$\frac{dP_b}{dz} = \alpha P_b h_{ab}(P_a - P_b) \qquad \text{mode b} \tag{1.48}$$

where

$$P_a = \frac{1}{2} e^{-az} \left(1 + e^{(-2h_{ab}z)} \right) \tag{1.49}$$

and

$$P_b = \frac{1}{2} e^{-az} \left(1 - e^{(-2h_{ab}z)} \right). \tag{1.50}$$

1.3.3 Frequency-dependent propagation model

An electric field propagating inside a fiber at frequency ω can be denoted as

$$E(x, y, z, \omega) = \sum_{u=1}^{M} A_u(z, \omega) E_u(x, y, \omega) \tag{1.51}$$

where $E_u(x, y, \omega) \quad u = 1, \cdots, M$ are the eigenmodes of the unperturbed fiber. The eigenmodes can be represented [12] by a vector as shown below.

$$\vec{\mathbf{A}}(z, \omega) = \left(A_1(z, \omega), A_2(z, \omega), A_3(z, \omega), \cdots, A_M(z, \omega) \right)^T \tag{1.52}$$

T indicating transpose. As seen previously in (1.28) describing the propagation in single mode regime, the linear propagation in multimode system is given by

$$\mathbf{A}(z, \omega) = \mathbf{F}(\omega) \mathbf{A}(0, \omega) \tag{1.53}$$

where $\vec{\mathbf{A}}(0, \omega)$ is the input field and $\vec{\mathbf{A}}(z, \omega)$ is the output field. $\mathbf{F}(\omega)$ is a F×F matrix that describes the evolution of the electric field from the input to the output. Such a matrix can be described by the wave plate model as the concatenation of K sections each of length L(k)

The equation describing uncoupled propagation in the kth section is given by

$$A_u(z,\omega) = \exp\left[\frac{-\alpha_u}{2}L^{(k)} - j\beta_u(\omega)L^{(k)}\right]A_u(0,\omega) \tag{1.54}$$

with the propagation constant β_u expanded using Taylor series to describe mode and chromatic dispersion. Mode dispersion is described by the uncoupled group delays

$$\beta_{1,u} = \frac{d\beta_u^k}{d\omega}(\omega) \qquad u = 1, \cdots, M. \tag{1.55}$$

The average uncoupled group delay is given by

$$\bar{\beta}_1^{(k)}L^{(k)} = \frac{L^{(k)}}{M}\sum_u \beta_{1,u}^{(k)} \tag{1.56}$$

and then mode dispersion is quantified using the parameter τ where

$$\tau_u = \beta_{1,u}^{(k)} - \bar{\beta}_1^{(k)} \tag{1.57}$$

and $\Sigma_u\tau_u = 0$. Vector τ describes the group delays in k-th section where

$$\tau^{(k)} = \left(\tau_1^{(k)}, \tau_2^{(k)}, \tau_3^{(k)}, \cdots, \tau_M^{(k)}\right). \tag{1.58}$$

Chromatic dispersion in the k-th section which is a combination of both waveguide and material dispersion is given by

$$\beta_{2,u}^k(\omega) = \frac{-\lambda^2}{2\pi c}D_u^k \qquad\qquad u = 1, \cdots, M \tag{1.59}$$

where $D_u^{(k)}$ is the dispersion coefficient of mode u given by

$$D_u^{(k)} = \frac{d\left(\frac{1}{V_{g,u}}\right)}{d\lambda} \tag{1.60}$$

and $V_{g,u}$ is the group velocity of its carrier wavelength. The mean mode chromatic dispersion parameter is denoted by

$$\bar{\beta}_2^{(k)} = \frac{1}{M}\sum_u \beta_{2,u}^{(k)} \tag{1.61}$$

and mode dependent chromatic dispersion is described by

$$\Delta\beta_{2,u}^{(k)} = \beta_{2,u}^{(k)} - \bar{\beta}_2^{(k)} \tag{1.62}$$

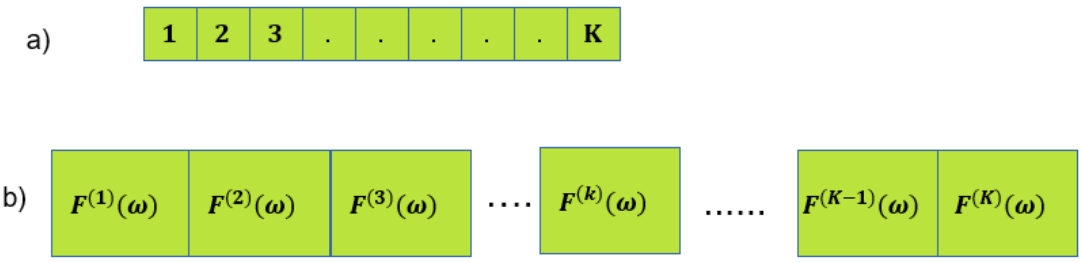

Figure 1.3: a) The division of the fiber into small sectionsof length L(k) b)Each section is decscribed by a propagation matrix F.

where

$$\sum_u \Delta\beta_{2,u}^{(k)} = 0 \tag{1.63}$$

as shown in [12].

It is also possible to include mode dependent loss in the k-th section by a vector g^k with the vector being given as

$$g^{(k)} = \left(g_1, g_2, g_3, \cdots, g_M \right) \tag{1.64}$$

where

$$g_u^{(k)} = -\left(\alpha_u^{(k)} - \bar{\alpha}^{(k)} \right) L^{(k)} \tag{1.65}$$

and

$$\sum_u g_u^{(k)} = 0 \tag{1.66}$$

with the average attenuation constant being calculated as:

$$\bar{\alpha} = \frac{1}{M} \sum_u \alpha_u \qquad\qquad u = 1, \cdots, M \tag{1.67}$$

As shown in [12], the equation describing uncoupled linear propagation in the k-th section including mode dependent loss, mode dependent chromatic dispersion and mode dispersion is:

$$\Lambda^{(k)}(\omega) = \begin{pmatrix} e^{\frac{1}{2} g_1^{(k)} - j\omega\tau_1^{(k)} - \frac{j}{2}\omega^2 \Delta\beta_{2,1} L^{(k)}} & \dots & 0 \\ \vdots & & \\ 0 & \dots & e^{\frac{1}{2} g_M^{(k)} - j\omega\tau_M^{(k)} - \frac{j}{2}\omega^2 \Delta\beta_{2,M} L^{(k)}} \end{pmatrix}. \tag{1.68}$$

Its customary to factor out the dispersion and the mode gain in (1.68) by

$$exp\left[\frac{1}{2}\bar{\alpha}^{(k)}L^{(k)} - j\bar{\beta}_1^{(k)}L^{(k)} - \frac{j}{2}\omega^2\bar{\beta}_2 L^{(k)}\right]. \tag{1.69}$$

The coupled linear propagation on the k-th section is described by

$$\mathbf{F}^{(k)}(\omega) = \mathbf{V}^{(k)}\mathbf{\Lambda}^{(\mathbf{k})}(\omega)\mathbf{U}^{(\mathbf{k})\dagger} \tag{1.70}$$

where $\mathbf{V}^{(k)}$ and $\mathbf{U}^{(k)}$ are frequency independent unitary matrices representing coupling at the input and output respectively. † denotes Hermitian transpose. When K sections of the fiber are concatenated together, the propagation equation modelled by the matrix is given by:

$$\mathbf{F}^{(t)}(\omega) = \mathbf{F}^{(K)}(\omega)\mathbf{F}^{(K-1)}(\omega)\mathbf{F}^{(K-2)}(\omega)\cdots\mathbf{F}^{(2)}(\omega)\mathbf{F}^{(1)}(\omega). \tag{1.71}$$

In strong coupling, the correlation length is shorter than the fiber length and hence the matrix propagation model requires the use of several fiber sections **K** with statically independent the unitary matrices $\mathbf{V}^{(k)}$ and $\mathbf{U}^{(k)}$ to ensure independence in each section. As previously seen in the single mode case but on a different scale for the multimode case, the eigenvalues describing the linear effects scale with the square root of the fiber length.

In weak coupling, the correlation length is usually smaller than fiber length. In this case the eigenvalues describing the linear effects scales proportionally with the length of the fiber.

1.4 Mode dispersion

Unlike in single mode fibers where polarization mode dispersion has a little or no effect and can be neglected, mode dispersion in multimode fibers cannot be neglected. It arises when spatial modes propagate with different group delays. Mode dispersion is particularly high in fibers with step index profiles, while it can be mitigated by using fibers with parabolic graded index profiles.

To understand the effect of mode coupling on mode dispersion, we assume that mode dependent loss is negligible. The above assumptions changes (1.71) to a M×M identity matrix as shown in [12] and given by

$$\mathbf{F}^{(t)*}(\omega)\mathbf{F}^{(t)}(\omega) = \mathbf{I} \tag{1.72}$$

where **I** is a MXM identity matrix.

Defining

$$\mathbf{G} = j\mathbf{F}_{\omega}^{(t)}\mathbf{F}^{(t)*}(\omega) \tag{1.73}$$

as a group delay operator where

$$\mathbf{F}_{\omega}^{(t)} = \frac{d\mathbf{F}^{(t)}(\omega)}{d\omega} \tag{1.74}$$

is the differentiation with respect to ω. The input- output relationship of the k-th section is described by

$$A(z,\omega) = \mathbf{F}^{(k)}(\omega)A(0,\omega) \tag{1.75}$$

$$A(0,\omega) = \mathbf{F}^{(k)\dagger}(\omega)A(z,\omega) \tag{1.76}$$

$$\Lambda^{(t)}(\omega) = \begin{pmatrix} e^{-j\omega\tau_1} & & 0 \\ & \ddots & \\ 0 & & e^{-j\omega\tau_1} \end{pmatrix}. \tag{1.77}$$

The matrix shown on (1.77) describes the propagation of principal modes and since it is diagonal it only describes the differential delays and no distortions resulting from crosstalk.

Chapter 2

Nonlinear Propagation and Interference in Optical Fiber Systems

This chapter explains the non-linear propagation in optical fiber systems starting with its genesis in optical systems. The first part of the chapter describes the non-linear propagation and interferences in the scalar case while the second part extends the nonlinear propagation to the multimode scenario by discussing its propagations and effects.

2.1 Nonlinear propagation and Interference in Scalar Case

When the intensity of an electric field is increased, a dielectric material like an optical fiber produces a nonlinear response and as a result the polarization experienced on the material is not linear, but nonlinear [22]. It is described by:

$$\mathbf{P} = \varepsilon_0 \left(X^{(1)}\mathbf{E} + X^{(2)}\mathbf{EE} + X^{(3)}\mathbf{EEE} + \cdots \right) \tag{2.1}$$

where ε_0 is the permittivity in the vacuum, $X^{(1)}$ is the linear susceptibility representing the dominant contribution to polarization and it influences the refractive index and attenuation coefficient. $X^{(2)}$ is the second order susceptibility responsible for second harmonic generation. Second nonlinear effects vanish in materials with symmetric moleculars like the optical fibers. The third order susceptibility $X^{(3)}$ is responsible for third harmonic generation, four wave mixing, and non-linear refraction. As a consequence of $X^{(3)}$, the

resulting non-linear impairments show an intensity dependence on the refractive index. The refractive index can then be rewritten as

$$\tilde{n}(\omega, |E|^2) = n(\omega) + n_2|E|^2 \tag{2.2}$$

where $n(\omega)$ is the linear part given by Sellmeier equation, $|E|^2$ is the optical intensity inside the fiber, n_2 is the non-linear index coefficient related to third-order susceptibility by

$$n_2 = \frac{3}{8n}\mathrm{Re}(X_{xxxx}). \tag{2.3}$$

The nonlinear polarization vector in (2.1) can be rewritten [25] as:

$$\begin{aligned}\vec{P}_R(\vec{r},\tau) = \varepsilon_0 X_{el}^{(3)}|\vec{E}(\vec{r},t)|^2\vec{E}(\vec{r},t) + \varepsilon_0 X_R^{(3)}\int_{-\infty}^{\infty} d\tau(t-\tau)|\vec{E}(\vec{r},\tau)|^2\vec{E}(\vec{r},t) \\ +\varepsilon_0 X_{R,\perp}^{(3)}\int_{-\infty}^{\infty} d\tau g(t-\tau)\vec{E}(\vec{r},t)\vec{E}(\vec{r},\tau).\vec{E}(\vec{r},\tau).\end{aligned} \tag{2.4}$$

The first term to the left of (2.4) proportional to X_{el} defines the instantaneous electronic response in glass while the second and the third term defines the response of the nuclei. The third term results from nuclear response and since its magnitude is lower than the magnitude of the second term, it can be neglected. The effect on both the electrons and nuclei causes a contribution that propagates in the same direction as the existing field. The two terms $g(t)$ and $h(t)$ are assumed to be normalized to 1. Equation (1.34) becomes

$$\frac{d|\tilde{E}\rangle}{dz} = i\mathbf{B}|\tilde{E}\rangle - \mathbf{A}|\tilde{E}\rangle + |L^{(NL)}\rangle \tag{2.5}$$

where $|L^{(NL)}\rangle$ is a nonlinear term given by

$$L^{(NL)} = \frac{i\omega_0}{2N_n(\omega_0)}\int dxdy\bar{F}_n(x,y,\omega_0)\vec{P}_R(\vec{r},\tau). \tag{2.6}$$

By using (1.1) and (2.3) and following the steps of section 2.3 of [23], we get

$$\frac{dE}{dZ} = -\frac{\alpha}{2}A - \beta_1\frac{dE}{dt} + j\frac{\beta_2}{2}\frac{d^2E}{dt^2} + \frac{\beta_3}{6}\frac{d^3E}{dt^3} - \frac{j3\omega_0^2 X_{xxxx}}{8\beta_0 c^2}|E|^2E \tag{2.7}$$

an equation known as Non-linear Schroedinger equation (NLSE). The normalization used in (1.25) changes (2.7) and it becomes related to the instantaneous power by

$$\frac{dA}{dZ} = -\frac{\alpha}{2}A - \beta_1\frac{dA}{dt} + j\frac{\beta_2}{2}\frac{d^2A}{dt^2} + \frac{\beta_3}{6}\frac{d^3A}{dt^3} - j\gamma|A|^2A. \tag{2.8}$$

The effect of intensity on the refractive index results in two effects: self-phase modulation(SPM) and cross-phase modulation (XPM).

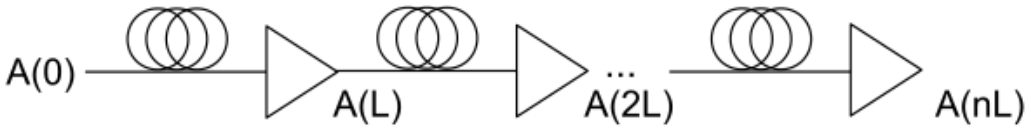

Figure 2.1: Multi-span fiber system

2.1.1 Self-phase modulation

Self-phase modulation is a nonlinear effect realized when an electric field induces a nonlinear phase shift when the field propagates inside an optical fiber. SPM is dominant when the nonlinear length L_{NL} is much less than the fiber length L and the fiber length is much less than the fiber dispersion length L_D.

$$L_{NL} << L << L_D. \tag{2.9}$$

Nonlinear length is calculated as $L_{NL} = \frac{1}{\gamma P}$ while the dispersion length is calculated as $L_D = \frac{T_0}{|\beta_2|^2}$ with T_0 being the symbol period. By using a pre-attenuated reference system where

$$A(z,t) = \sqrt{P}e^{-\frac{\alpha}{2}z}U(z,\tau), \tag{2.10}$$

its derivative $\frac{dA}{dz}$ is given by:

$$\frac{dA}{dz} = -j\gamma|A|^2Ae^{-\alpha z}. \tag{2.11}$$

Inverting (2.10), its derivative can be re-written as:

$$\frac{dU}{dz} = j\frac{sign(\beta_2)}{2L_D}\frac{d^2U}{d\tau^2} + \frac{sign(\beta_3)}{6L_D}\frac{d^3U}{d\tau^3} - j\frac{e^{-\alpha z}}{L_{NL}}|U|^2U. \tag{2.12}$$

Assuming no group velocity dispersion and third order dispersion, (2.12) reduces further to:

$$\frac{dU}{dz} = \frac{-j}{L_{NL}}|U|^2Ue^{-\alpha z}. \tag{2.13}$$

Let

$$A(z) = |A|e^{j\phi(z)} \tag{2.14}$$

be the phase component and using the equality

$$\frac{d|A|^2}{dz} = \frac{dAA^*}{dz} = A\frac{dA^*}{dz} + \frac{dA}{dz}A^* \tag{2.15}$$

and substituting the phase component in (2.14) into (2.11), we get the change of phase given by:

$$\frac{d\phi}{dz} = -\gamma|A|^2 e^{-\alpha z}. \tag{2.16}$$

After distance z, the phase change is given by:

$$\phi(z) = \phi(0) - \gamma \int e^{-\alpha \wr} d\wr \, |A(0)|^2, \tag{2.17}$$

thus a known electric field at $A(0)$ with $\phi(0)$ will experience a phase shift and the known electric field changes to

$$A(z) = |A(0)|e^{j[\phi(0)-\gamma|A(0)|^2 L_{eff}(z)]} \tag{2.18}$$

after distance z. L_{eff} is the effective length given by

$$L_{eff} = \int e^{-\alpha \wr} d\wr = \frac{1 - e^{-\alpha z}}{\alpha}. \tag{2.19}$$

SPM exists in the first few kilometres of the fiber and the nonlinear phase rotation at any distance z, is given by

$$\phi_{NL} = \gamma|A(0)|^2 L_{eff}(z). \tag{2.20}$$

For a multi-span system as shown in figure 2.1, SPM grows with the number of spans. For example after span 1, the SPM is

$$A(L) = |A(0)|e^{j\gamma|A(0)|^2 L_{eff}(z)} \tag{2.21}$$

After span 2,

$$A(2L) = |A(0)|e^{j2\gamma|A(0)|^2 L_{eff}(z)} \tag{2.22}$$

After n spans,

$$A(nL) = |A(0)|e^{jn\gamma|A(0)|^2 L_{eff}(z)}. \tag{2.23}$$

2.1.2 Cross-phase modulation

To increase the capacity, wavelength division multiplexing is used where two channels or more are propagated inside the fiber at different wavelengths. However because of Kerr effects, they interact with each other causing nonlinear cross talk.

Consider two channels, a and b, with different fields. In the absence of group velocity dispersion and four wave mixing, their propagation equations are:

$$\frac{dA_a}{dz} = -\frac{\alpha}{2}A_a - \beta_{1a}\frac{dA_a}{dt} - j\gamma|A_a|^2 A_a - j2\gamma|A_b|^2 A_a \qquad \text{Channel a} \tag{2.24}$$

$$\frac{dA_b}{dz} = -\frac{\alpha}{2}A_b - \beta_{1b}\frac{dA_b}{dt} - j\gamma|A_b|^2 A_b - j2\gamma|A_a|^2 A_b \qquad \text{Channel b.} \tag{2.25}$$

After a change of variable in the retarded time frame of channel a, (2.24) and (2.25) can be rewritten as:

$$\frac{dA_a}{dz} = -\frac{\alpha}{2}A_a - j\gamma|A_a|^2A_a - j2\gamma|A_b|^2A_a \tag{2.26}$$

and

$$\frac{dA_b}{dz} = -\frac{\alpha}{2}A_b - (\beta_{1b} - \beta_{1a})\frac{dA_b}{dt} - j\gamma|A_b|^2A_b - j2\gamma|A_a|^2A_b. \tag{2.27}$$

Again in a lossless reference system:

$$A_{a,b}(z,\tau) = e^{-\frac{\alpha}{2}z}U_{a,b}(z,\tau) \tag{2.28}$$

we get

$$\frac{d|U_a|^2}{dz} = U_a^*\frac{dU_a}{dz} + \frac{dU_a^*}{dz}U_a = 0 \tag{2.29}$$

hence, the power is not changing contrary to the phase. For channel b we have:

$$\frac{d|U_b|^2}{dz} = U_b^*\frac{dU_b}{dz} + \frac{dU_b^*}{dz}U_b = d_{ab}U_b^*\frac{dU_b}{dz} + d_{ab}\frac{dU_b^*}{dz}U_b \tag{2.30}$$

where $d_{ab} = \beta_{1a} - \beta_{1b}$. Equation (2.30) can be solved exactly showing a channel walk-off

$$|U_b(z,\tau)|^2 = |U_b(0,\tau + d_{ab}z)|^2. \tag{2.31}$$

Applying the same procedure as done in section 2.1.1 for SPM, we get the change of phase as:

$$\frac{d\phi_a}{dz} = -\gamma e^{-\alpha z}|U_a(0,\tau)|^2 - 2\gamma e^{-\alpha z}|U_b(z,\tau)|^2 \tag{2.32}$$

where $|U_b(z,\tau)|^2 = |U_b(0,\tau + d_{ab}z)|^2$. By integrating both sides of (2.32), the result is

$$\phi_a(z,\tau) = \phi_a(0,\tau) - \gamma\int_0^z e^{-\alpha\xi}|U_a(0,\tau)|^2d\xi - 2\gamma\int_0^z e^{-\alpha\xi}|U_b(0,\tau + d_{ab}\wr)|^2d\xi. \tag{2.33}$$

The first term of the right hand part of (2.33) is the phase change resulting from SPM, while the second term is caused by XPM. In WDM systems, XPM is usually stronger than in fully loaded WDM systems. Moreover while SPM is memoryless, XPM does have a memory.

2.1.3 Four wave mixing

Four wave mixing (FWM) results when three electric fields propagate inside the fiber simultaneously, such that a fourth field at frequency ω_4 is generated resulting from the third order susceptibility discussed in (2.1). The frequency generated is related to the other three fields by:

$$\omega_4 = \omega_1 + \omega_2 \pm \omega_3 \tag{2.34}$$

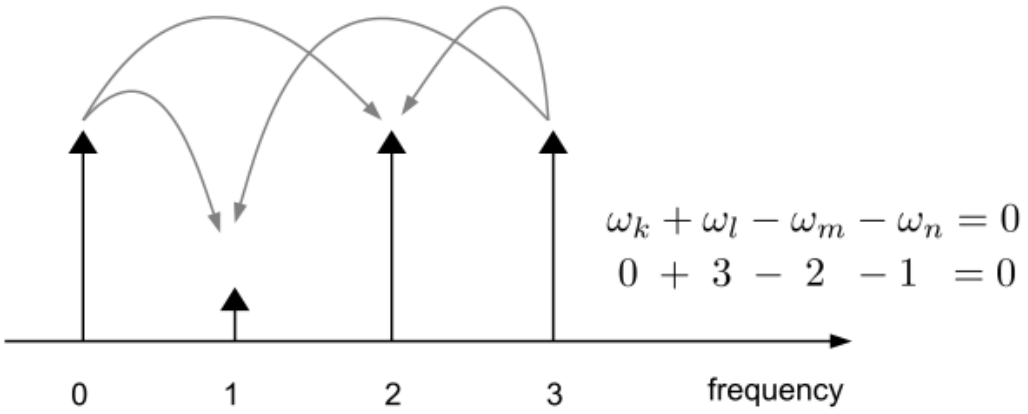

Figure 2.2: Four wave mixing: showing energy transfer between the channels [23].

FWM is dominant when the channel spacing and the dispersion are small, satisfying the phase match condition. To understand the phase matching condition, we use regular perturbation method [24] to solve the NLSE. Equation (2.8) can be rewritten as

$$\frac{dA_n}{dZ} = -\frac{\alpha}{2}A_n - \beta_{1,n}\frac{dA}{dt} + j\frac{\beta_2}{2}\frac{d^2A_n}{dt^2} + \frac{\beta_3}{6}\frac{d^3A_n}{dt^3} - j\gamma\Sigma_{k,l,m}A_kA_lA_m^*e^{-j\Delta\beta_{klm}z}. \quad (2.35)$$

The idea of regular perturbation is solving the NLSE by assuming that the γ is very small. We let $A_n(z,t)$ to be the function of γ as:

$$A_n(z,t) = f(\gamma, A_n, \forall n). \quad (2.36)$$

Equation (2.36) can be expanded by using Taylor series to get

$$A_n(z,t) = \sum_{p=0}^{\infty} A_{np}(z,t)\gamma^p \quad (2.37)$$

where p denotes the perturbation order and n the channel number. By substituting the expanded Taylor series into (2.35), we find

$$\begin{aligned}\sum_{p}^{\infty}\frac{dA_{np}}{dz}\gamma^p = \sum_{p=0}^{\infty}\left\{-\frac{\alpha}{2}A_{np} - \beta_{1n}\frac{dA_{np}}{dt} + j\frac{\beta_{2n}}{2}\frac{d^2A_{np}}{dt^2}\right\}\gamma^p \\ -j\sum_{p,q,s=0}^{\infty}\sum_{klm}\gamma^{p+q+s+1}A_{kp}A_{lq}A_{ms}^*e^{-j\Delta\beta_{klm}z}.\end{aligned} \quad (2.38)$$

To get the unperturbed signal we set p=0, and get an input-output relation as was shown in (1.28) in Chapter 1 related to:

$$A_{n0}(z,t) = A(0,t). \quad (2.39)$$

For p=1, the perturbation solution is given by:

$$\frac{dA_{n1}}{dz} = \left\{ -\frac{\alpha}{2}A_{n1} - \beta_{1n}\frac{dA_{n1}}{dt} + j\frac{\beta_{2n}}{2}\frac{d^2A_{n1}}{dt^2} \right\} - A_{k0}A_{l0}A^*_{m0}e^{-j\Delta\beta_{klm}z}. \tag{2.40}$$

By using the boundary condition $A_{n1}(z,t) = 0$, and assuming constant waves in the pre-attenuated reference system, (2.40) changes to

$$\frac{dU_{n1}}{dz} = -je^{-\alpha z}\sum_{klm} U_k U_l U_m e^{-j\Delta\beta_{klm}z}. \tag{2.41}$$

Such equation can be solved exactly yielding:

$$\int_0^z \frac{dU_{n1}}{dz} = U_{n1}(z) - U_{n1}(0) = -je^{-\alpha z}\sum_{klm} U_{k0}U_{l0}U_{m0}e^{-j\Delta\beta_{klm}z}. \tag{2.42}$$

hence

$$U_{n1}(z) = -j\sum_{klm} U_{k0}U_{l0}U_{m0}\int_0^z e^{-\alpha\xi}e^{-j\Delta\beta_{klm}\xi}d\xi \tag{2.43}$$

In a single mode fiber, the integral can be closed yielding a FWM kernel given by:

$$\eta_{klmn} = \frac{1 - e^{-\alpha z}e^{-j\Delta\beta_{klm}z}}{\alpha + j\Delta\beta_{klm}} \tag{2.44}$$

where $\Delta\beta_{klm}$is the phase matching coefficient given by

$$\Delta\beta_{klm} = \beta(\omega_k) + \beta(\omega_l) - \beta(\omega_m) = \beta(\omega_n). \tag{2.45}$$

Knowing that $U_n(z) = U_{n0} + \gamma U_{n1}$ and replacing the derivations in the main equation, we find that the effect of FWM is given by:

$$A_n(z) = e^{\frac{\alpha}{2}z}\left[A_n(0) - j\gamma\sum_{klm} A_{k0}(0)A_{l0}(0)A^*_{m0}(0)\eta_{klmn} \right]. \tag{2.46}$$

As a general observation, we note that FWM can be reduced through bigger group velocity dispersion values and unequal spacing between the channels, if possible.

2.2 Nonlinear propagation in Mode Multiplexed Systems

Consider a fiber experiencing random coupling and supporting N spatial modes with the total number of scalar modes being 2N, the coupled nonlinear Schrödinger equation is given by

$$\frac{dE}{dz} = i\mathbf{B}^{(0)}E - \mathbf{B}^{(1)}\frac{dE}{dt} - i\mathbf{B}^{(2)}\frac{d^2E}{dt^2} + i\gamma\sum_{jhkm} C_{jhkm}E^*_h E_k E_m \tag{2.47}$$

where C_{jhkm} is the nonlinear coupling coefficient and is given [26] by

$$C_{jhkm} = \frac{n_{neff}^2 A_{11}}{N_j N_h N_k N_m} \times \left[\frac{2}{3} \int dxdy (F_j^* F_m)(F_h^* F_k) + \frac{1}{3} \int dxdy (F_j^* F_h^*)(F_m F_k) \right] \quad (2.48)$$

where $N_i^2 = \int dxdy|F_i|n_f$, while $i = j, h, k, m$ and n_f is the linear refractive index profile. Let $\gamma = \frac{\omega_0 n_2}{cA_{11}}$ be the nonlinear coefficient with c is the speed of light in vacuum. The effective area of the fundamental mode A_{11} is given by:

$$A_{11} = \frac{\left[\int dxdy|F_1|^2 \right]^2}{\int dxdy|F_1|^4}. \quad (2.49)$$

For the fundamental mode, the nonlinear coupling coefficient given by $c_{1111} = 1$. $N_1^2 = n_{eff} \int dxdy|F_1|^2$ where n_{eff} is the effective index of the fundamental mode.

The propagation of electric field of group a and group b are described by:

$$\frac{d\vec{E}_a}{dZ} = -\frac{\alpha}{2}\vec{E}_a + i\beta_a \vec{E}_a - \beta_a' \frac{d\vec{E}_a}{dt} - \mathbf{B}_a \frac{d\vec{E}_a}{dt} - i\frac{\beta_a''}{2}\frac{d^2\vec{E}_a}{dt^2} + i\gamma(K_{aa}|\vec{E}_a|^2 + K_{ab}|\vec{E}_b|^2)\vec{E}_a \quad \text{group a} \quad (2.50)$$

$$\frac{d\vec{E}_b}{dZ} = -\frac{\alpha}{2}\vec{E}_b + i\beta_b \vec{E}_b - \beta_b' \frac{d\vec{E}_b}{dt} - \mathbf{B}_b \frac{d\vec{E}_b}{dt} - i\frac{\beta_b''}{2}\frac{d^2\vec{E}_b}{dt^2} + i\gamma(K_{ba}|\vec{E}_a|^2 + K_{bb}|\vec{E}_b|^2)\vec{E}_b \quad \text{group b} \quad (2.51)$$

where $\mathbf{B}_a$ and $\mathbf{B}_b$ are 2×2 matrices that describe the birefringence experienced within the fiber. β_a'' and $\beta_b''$are the chromatic dispersion coefficients and β_a' and β_b' are the inverse group velocities. The term K_{uv} is a generalized SPM and XPM coefficient given by

$$K_{uv} = \sum_{k,m} \sum_{h \forall v} C_{jhkm} \frac{\delta_{hk}\delta_{jm} + \delta_{hm}\delta_{jk}}{2N_u + (2N_v + \delta_{vu})} \quad (2.52)$$

with δ_{ab} indicating the Kronecker delta.

Consider a wavelength division multiplexed signal in which we express the signal in group a as:

$$E_a = \sum_k E_{a,k} e^{-ik\Omega t} \quad (2.53)$$

and group b:

$$E_b = \sum_k E_{b,k} e^{-ik\Omega t} \quad (2.54)$$

where $\Omega/2\pi$ is the channel spacing. Let channel $E_{a,0}$ be the channel of interest and the remaining channels in both group a and group b be the interfering channels, i.e $E_{a,k}$ $k \neq 0$ and $E_{b,k}$ are the interfering channels.

Substituting (2.53) into (2.50) an intra-group interference arises from a term:

$$i\gamma K_{aa}(E^{\dagger}_{a,l}E_{a,m}E_{a,l-m} + \eta_{l,m}E^{\dagger}_{a,l}E_{a,l-m}E_{a,m}). \tag{2.55}$$

The coefficient $\eta_{l,m}$ is equivalent to 1 in all other cases except when $l = 2m$ or when $l = m = 0$ then it is 0. When (2.54) is substituted into (2.51), an inter-group interference equation is defined, given by:

$$i\gamma K_{ab}E^{\dagger}_{b,l}E_{a,l-m}E_{a,m} \tag{2.56}$$

As was done in [27], mode dispersion is assumed to be sufficiently large such that the channels in the WDM system undergo independent mode coupling. Moreover we assume that the distortion caused within the individual channels is negligible [1] .

2.2.1 Intra-group nonlinear interference

Intra-channel interaction

When $l = m = 0$ we have intra-channel effects. Equation (2.55) changes to:

$$i\gamma K_{aa}E^{\dagger}_{a,0}E_{a,0}E_{a,0,j} = i\gamma K_{aa}|E_{a,0,j}|^2E_{a,0,j} + i\gamma K_{aa}\sum_{k\neq j}^{2N_a}|E_{a,0,j}|^2E_{a,0,j} \tag{2.57}$$

where j is the j-th component of $E_{a,0}$. The first term on the right hand side of (2.57) is equivalent to the SPM in the scalar case as was defined in section 2.1.1. The other remaining term on the right hand side contributes to cross-phase modulation and is contributed by $2N_a - 1$ scalar modes and since they are statistically independent, their contributions to the interference can be summed. As was first shown in [27], we generalize all the SPM contribution by:

$$\sigma^2_{spm} = \sigma^2_{spm,0} + (2N_a - 1)(\sigma^2_{spm,1} - \sigma^2_{spm,0}) \tag{2.58}$$

where $\sigma^2_{spm,0}$ is the SPM due to the scalar case and $\sigma^2_{spm,1}$ is the generalized SPM governed by the Makanov equation given by:

$$\frac{dE}{dz} = -\frac{\alpha}{2}E - j\frac{\beta''}{2}\frac{d^2E}{dt^2} + i\frac{8}{9}\gamma|E|^2. \tag{2.59}$$

Two-channel interaction

Consider a two channel interaction as shown in fig. 2.3c where $l = m$, with $l, m \neq 0$. Equation (2.55) becomes

$$i\gamma K_{aa}\left(|E_{a,l}|^2\mathbf{I}_a + E_{a,l}E^{\dagger}_{a,l}\right)E_{a,0} \tag{2.60}$$

[1] hence we assume that the bandwidth of modal dispersion is smaller than the channel bandwidth.

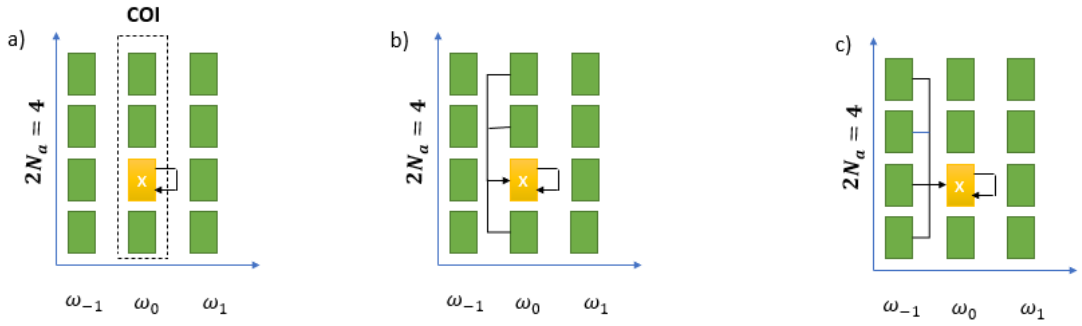

Figure 2.3: a) Shows 4 modes in the channel of interest(COI) and SPM resulting from the mode of interest. b) Shows cross phase modulation from different modes on the mode of interest; generalized as SPM since we are interested on the COI. c) Cross phase modulation from other channel different from COI.

where $\mathbf{I}_a$ is $2N_a \times 2N_a$ identity matrix. In the presence of large mode dispersion, (2.60) shown in [27] changes to:

$$i\gamma K_{aa}\left(1+\frac{1}{2N_a}\right)|E_{a,l}|^2 E_{a,0}. \tag{2.61}$$

If the jth component of vector $E_{a,l}$ is considered, (2.61) can be rewritten as

$$i\gamma K_{aa}\left(1+\frac{1}{2N_a}\right)\sum_k |E_{a,l,k}|^2 E_{a,0,j}. \tag{2.62}$$

The modes provide $2N_a$ statistically independent nonlinear contributions and thus the total XPM interference induced on the channel of interest is the sum of the individual contributions and is given by:

$$\sigma^2_{xpm} = 2N_a\left(1+\frac{1}{2N_a}\right)^2 \frac{\sigma^2_{xpm,scalar}}{4}\frac{(2N_a+1)^2}{8N_a} \tag{2.63}$$

where $\sigma^2_{xpm,scalar}$ is the variance produced by a single channel as in WDM as shown in the scalar case. The factor of 4 shown in the equation accounts for the factor 2 present in XPM in the scalar case.

When mode dispersion is small, the intra-group interference can be written as:

$$2i\gamma K_{aa}|E_{a,l,j}|^2 E_{a,0,j} + i\gamma K_{aa}\sum_{k\neq j}|E_{a,l,k}|^2 E_{a,0,j} + i\gamma K_{aa}\sum_{k\neq j} E_{a,l,j}E_{a,l,k}E_{a,0,k} \tag{2.64}$$

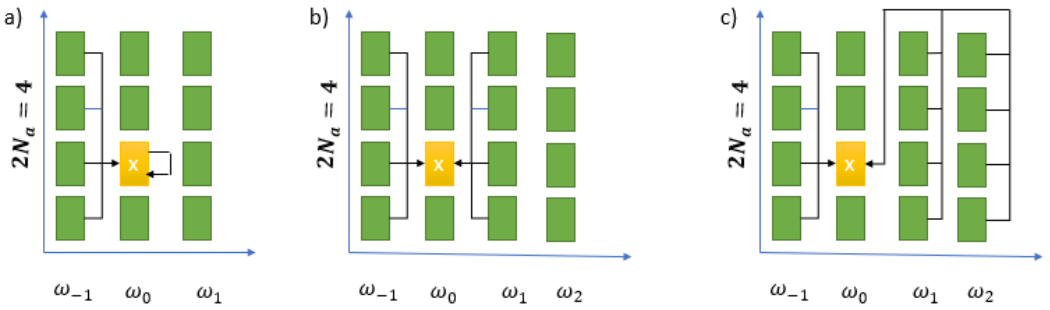

Figure 2.4: a) Two channel interaction b) Three channel interaction with two channels being degenerate to the COI. c) Four channel interaction

where the first term is similar to the XPM variance given in the scalar case after replacing $\gamma \rightarrow \gamma K_{aa}$. The other $2N-1$ contributions represented by the summations in the equation, yield an XPM variance

$$\sigma^2_{xpm} = \sigma^2_{xpm,scalar} + \Big(2N_a - 1\Big)\Big(\sigma^2_{xpm,0} - \sigma^2_{xpm,scalar}\Big) \tag{2.65}$$

where $\sigma^2_{xpm,0}$ is the XPM variance in each of the two polarizations of the single mode fiber obeying Manakov equation.

Three-channel interaction

This interaction occurs when two interfering channels imposes effects on the channel of interest. When mode dispersion is large enough the channels undergo uncorrelated random coupling and thereby the nonlinear effects build up incoherently and can be neglected, therefore, we only consider the case when mode dispersion is at a low value.

Three channel interaction exists in two forms; in one form, one channel is degenerate to the channel of interest while in the second form, one channel is degenerate with respect to one of the interfering channels. In the first case, the intra-group interference experienced by channel 0 is given by:

$$i\gamma K_{aa} E^*_{a,0} E_{a,m} E_{a,-m} + i\gamma K_{aa} E^*_{a,0} E_{a,-m} E_{a,m} \tag{2.66}$$

with $m \neq 0$. Its j-th component is expressed by:

$$i\gamma K_{aa}\left(2E^*_{a,0,j} E_{a,m,j} E_{a,-m,j} + \sum_{k\neq j} E^*_{a,0,k} E_{a,m,k} E_{a,-m,j} + E^*_{a,0,k} E_{a,-m,k} E_{a,-m,j}\right) \tag{2.67}$$

All terms in (2.67) are independent of each other and thus their contributions are summed to get the total interference given by:

$$\sigma^2_{3-I} = \frac{(2N_a+1)}{2}\sigma^2_{3-I,scalar} \tag{2.68}$$

where $\sigma^2_{3-I,scalar}$ is the nonlinear interference resulting from three channel interaction in the single mode case.

In the second case, the intra-group interference is given by:

$$i\gamma K_{aa} E^*_{a,2m} E_{a,m} E_{a,m} \tag{2.69}$$

where $m \neq 0$. When $l = 2m$, its jth component is denoted by:

$$i\gamma K_{aa} E^*_{a,2m,j} E^2_{a,m,j} + i\gamma K_{aa} \sum_{k,k\neq j} E^*_{a,2m,k} E_{a,m,k} E_{a,m,k} \tag{2.70}$$

where the first term of the equation is equivalent to the nonlinear variance from the scalar case and the remaining terms is same as the $2N_a - 1$. All in all, the nonlinear variance can be written as

$$\sigma^2_{3-II} = \sigma^2_{3-II,scalar} + \left(2N_a - 1\right)\left(\sigma^2_{3-II,0} - \sigma_{3-II,scalar}\right) \tag{2.71}$$

where $\sigma_{3-II,scalar}$ is the three channel nonlinear variance resulting from the scalar case and $\sigma_{3-II,0}$ three channel nonlinear variance from the single mode case.

Four-channel interaction

Occurs when three channels interact with the channel of interest and as shown in fig. 2.4c, the nonlinear interference is described by:

$$i\gamma K_{aa} E^*_{a,l} E_{a,m} E_{a,l-m} + i\gamma K_{aa} E^*_{a,l} E_{a,l-m} E_{a,m} \tag{2.72}$$

where $l \neq m$, $l \neq 2m$ and $l, m \neq 0$. Its jth component is given by:

$$i2\gamma E^*_{a,l,j} E_{a,m,j} E_{a,l-m,j} + i\gamma K_{aa} \sum_{k,k\neq j} E^*_{a,l,k} E_{a,m,k} E_{a,l-m,j} + E^*_{a,l,k} E_{a,l-m,k} E_{a,m,j}. \tag{2.73}$$

Since all the terms are uncorrelated and independent, the nonlinear variance arising from the four channel interaction is given by

$$\sigma^2_{4ch} = \frac{2N_a+1}{2}\sigma^2_{4ch,scalar}. \tag{2.74}$$

Mode dispersion is beneficial in combating nonlinear interference in fact in the presence of large mode dispersion, three and four channels interactions are averaged out because of the uncorrelated wavelength multiplexed channel during propagation. For example, in the experiment done by [27], the authors showed that the effect of XPM can be reduced efficiently if a large value of mode dispersion is allowed.

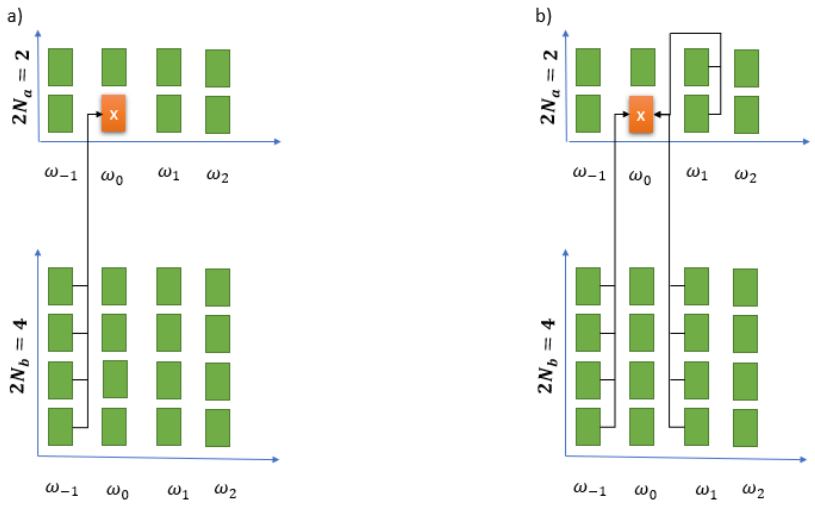

Figure 2.5: a) Inter-group interference between two groups similar to XPM. b) Inter-group interference similar to four wave mixing-in both cases we assume that receiver processes the signal independently and thus the zero frequency at group a and at group b can be processed independently.

2.2.2 Inter-group nonlinear interference

Consider two groups of modes; group a with $2N_a$ spatial modes and group b with $2N_b$ spatial modes. Let group a, have the channel of interest and thus inter-group nonlinear interference is the effects imposed on the COI by the channels in group b. The nonlinear effects is defined by

$$i\gamma K_{ab} E^*_{a,l} E_{b,m} K_{a,l-m} \tag{2.75}$$

and it exists in two forms when $l = m$ and $l \neq m$.

a) Degenerate case $l = m$

When $l = m$, (2.75) changes to

$$i\gamma K_{ab} |E_{b,0}|^2 E_{a,0} \tag{2.76}$$

and its vector expressed as:

$$i\gamma K_{ab} \sum_k |E_{b,l,k}|^2 E_{a,0}. \tag{2.77}$$

The channels in group b impose cross-group phase modulation denoted by

$$\sigma_{\text{XGXPM}} = 2N_b \zeta_{xpm,scalar} \tag{2.78}$$

$\zeta_{xpm,scalar}$ is similar to $\sigma_{xpm,scalar}$ shown in the previous section, with the difference that the group velocities and chromatic dispersions must be accounted for as shown in [27].

b)Non degenerate case $l \neq m$

With this condition, (2.75) changes to

$$i\gamma K_{ab} E^*_{b,l} E_{b,l} E_{a,l-m} \tag{2.79}$$

which is equivalent to four wave mixing in intra-group interference and hence in the presence of large mode dispersion this effect is negligible. On the other hand when mode dispersion is negligible then this effect must be accounted for. Its contribution is denoted by:

$$\sigma_{xGfwm} = 2N_b \zeta_{4ch,scalar} \tag{2.80}$$

where $\zeta_{4ch,scalar}$ is similar to the nonlinear interference contributed by the four channel interaction as was seen in the intra-group interference with the exception that the channels are experiencing different chromatic dispersion and group velocities.

Chapter 3

Simulation Results and Discussion

In this chapter, we investigate the effects of mode dispersion in the nonlinear regime by simulating different optical fiber scenarios. Firstly, we investigate the nonlinear optical system response in the single mode fibers when the value of polarization mode dispersion is varied. Secondly, we investigate the nonlinear optical system response in the SDM case when the number of modes and the value of mode dispersion is varied. The investigation is done both by the split step Fourier method (SSFM) simulations and the Gaussian noise model that was extended in [28] to accommodate mode dispersion.

3.1 Gaussian noise model

The variance of the nonlinear interference can be computed through the Gaussian noise model [29]. By using this model we assume that the transmitted signal is Gaussian distributed and that the nonlinear impairments received are additive as per the additive white Gaussian noise channel. The signal to noise ratio (SNR) can thus be defined as:

$$SNR = \frac{P_s}{P_{ASE} + P_{NLI}} \tag{3.1}$$

where P_{ASE} is the power of amplified spontaneous emission, P_{NLI} is the power arising from the non-linear impairments and P_s is the power of the signal transmitted in the fiber. The SNR penalty due to the nonlinear interference is given by:

$$SNR = \frac{P_s}{P_{ASE}} \frac{1}{1 + \frac{P_{NLI}}{P_{ASE}}} = \frac{SNR_{lin}}{SP} \tag{3.2}$$

where SP is the penalty with respect to the linear propagation. The additive NLI is reasonably a circular noise, with a small phase noise contribution that in most of the links has a minor impact [30]. The power spectral density of the NLI can be evaluated according to the GN model, whose main result when the transmitted symbols are Gaussian

distributed is:

$$G_{NLI}(f) = \frac{16}{27}\gamma^2 L_{eff}^2 \int_{-\infty}^{\infty}\int_{-\infty}^{\infty} G_{WDM}(f_1)G_{WDM}(f_2)G_{WDM} \\ (f_1+f_2+f_3)\rho(f_1,f_2,f)\chi(f_1,f_2,f)df_2df_1 \tag{3.3}$$

where

1. γ is the nonlinear coefficient.
2. L_{eff} is the effective length in kilometres.
3. $G_{WDM}(f)$ is the WDM signal power spectral density.
4. $\rho(f_1, f_2, f)$ is the FWM efficiency.
5. $\chi(f_1, f_2, f)$ is the coherent interference at the receiver that takes into account multiple spans.

The formula can be interpreted as a description of the beating between a single WDM signal with all other signals through a FWM process. The beating process as a result, introduces interferences which can be classified as: self-channel interference, cross-channel interference, and multi-channel interference.

The power spectral density of nonlinear interference is reasonably flat within the signal bandwidth. Its value at the spectrum $f = 0$, has been approximated by Poggiolini [29] in a single span as:

$$G_{NLI}(0) = \frac{8}{27}\frac{\gamma^2 G_{WDM}^2 L_{eff}^2}{\pi\beta_2 L_{eff,a}}\text{asinh}\left(\frac{\pi^2}{2}\beta_2 L_{eff,a} B_{ch}^2 N_{ch}^{\frac{2B_{ch}}{\Delta f}}\right) \tag{3.4}$$

where B_{ch} is the bandwidth of the channel, N_{ch} is the number of channels, Δf is the channel spacing, $L_{eff} = (1 - exp(-\alpha L_s)/\alpha)$ is the effective length, L_s is the fiber length and $L_{eff,a} = 1/\alpha$.

For a multi-span system, the interference is calculated as:

$$G_{NLI} = \frac{16}{27}\frac{\gamma^2 L_{eff}}{\pi\beta_2 L_s}[1 - N_s + N_s \text{HarNum}(N_s - 1)] \tag{3.5}$$

where N_s is the number of spans, while HarNum(k) is the k-th harmonic number.

In a generalized and more accurate formula, according to [29], the nonlinear interferences due to XPM only can be calculated by:

$$G_{NLI}(0) = \frac{\gamma^2 G_{WDM}^3 L_{eff}^2 (\frac{2}{3})^3}{\pi\beta_2 L_{eff,a}}\left(\sum_{k=-\frac{Nch-1}{2},k\neq 0}^{\frac{Nch-1}{2}} [\text{asinh}(\pi\beta_2 L_{eff,a} B_{ch} \times [k\Delta f + \frac{B_{ch}}{2}]) \quad + \right. \\ \left. \text{asinh}(\pi\beta_2 L_{eff,a} B_{ch} \times [k\Delta f - \frac{B_{ch}}{2}])] + \text{asinh}(\frac{\pi}{2}\beta_2 L_{eff,a} B_{ch}^2)\right) \tag{3.6}$$

The Gaussian noise model was initially introduced for single mode fibers [29], [32]. It was later extended to include polarization dependent loss in [33]. In [34], [35] it was extended to include the non-linearities in the multimode and multicore scenarios. However, all such works neglected the interaction of mode dispersion with the Kerr effects. Unfortunately, mode dispersion cannot be neglected in the SDM case because of its high values and therefore it was included in the GN model by P. Serena, *et, al.* The authors in [28] focused mainly on the interaction with cross-phase modulation which is the dominant nonlinear effect in dense wideband communication systems.

The key idea of [28] was the following: consider a data symbol a_k at discrete time k_1 sent at channel k_2 on spatial mode k_3. The sent signal can be written as

$$|A\rangle = \sum_k a_k |G_k(0,t)\rangle \tag{3.7}$$

where

$$|G_k(0,t)\rangle = p(t - k_1 T) e^{j\Omega_{k_2} t} |k_3\rangle. \tag{3.8}$$

T is the symbol time, p the supporting pulse, Ω_{k_2} is the carrier frequency of the channel k_2. The interaction of the channel noise and the signal can be written as:

$$y_i = a_i + n_i \equiv a_i - j \sum_{k,m,n} a_k^* a_m a_n X_{kmni}. \tag{3.9}$$

X_{kmni} is defined as:

$$X_{kmni} = \gamma\kappa \int_0^z f(\xi) \langle G_k(\xi,t) | G_m(\xi,t)\rangle \times \langle G_i(\xi,t) | G_n(\xi,t)\rangle d\xi \tag{3.10}$$

where γ is the nonlinear coefficient, κ is the Manakov correction term given by [25]

$$\kappa = \frac{4}{3}\frac{2N}{2N+1}, \tag{3.11}$$

$f(z)$ is the loss function. As shown in [28], the variance of the nonlinear interference becomes:

$$var(n_1) = \sum_{k,m,n} \left(X_{kmni} X_{kmni}^* + X_{kmni} X_{knmi}^* \right). \tag{3.12}$$

In the absence of mode dispersion, the function X_{kmni} is symmetric to X_{knmi} yielding the factor 2 of classical XPM. The symmetry does not hold in the presence of mode dispersion.

In [28] the authors included mode dispersion in the XPM variance expression, under the assumption that intra-channel PMD can be neglected. As a consequence, only inter-channel PMD is taken into account. The idea is sketched in fig. 3.1. The Gaussian noise model can be extended to calculate the variance of XPM in a two channel scenario with ultra-long span length, as follows:

$$\lim_{L_s \to \infty} \sigma_{\text{xpm}}^2 = \frac{2N+1}{2N} \left((2N+1)\sigma_{\text{xpm},1}^2 + \frac{(2N-1)(\alpha + \frac{\Delta\omega^2\mu^2}{N})}{\alpha} \sigma_{\text{xpm},1}^2 \left(\alpha + \frac{\Delta\omega^2\mu^2}{N} \right) \right) \tag{3.13}$$

where N is the number of modes, $\sigma^2_{\text{xpm},1}$ is the XPM variance in the scalar case, μ is the mode delay and $\Delta\omega$ is the channel spacing. In the special case of dual polarization, mode delay μ is related to polarization mode dispersion value by

$$\mu = PMD\sqrt{\frac{\pi}{8}}. \tag{3.14}$$

$\sigma^2_{\text{xpm},1}$ is calculated by:

$$\sigma^2_{\text{xpm},1} = \frac{\gamma^2 \frac{P_{test}P^2_{int}}{R^3} L^2_{eff}(\frac{2}{3})^3}{\pi\beta_2 L_{eff,a}} \times \sum_{k=-\frac{Nch-1}{2},k\neq 0}^{\frac{Nch-1}{2}} \Bigg(\text{asinh}(\pi\beta_2 L_{eff,a} B_{ch} \times [k\Delta f + \frac{B_{ch}}{2}]) + \text{asinh}(\pi\beta_2 L_{eff,a} B_{ch} \times [k\Delta f - \frac{B_{ch}}{2}]) \Bigg) \times R \tag{3.15}$$

where R is the symbol rate, P_{test} is the power of the channel under test and P_{int} is the power of the interfering channel.

3.2 Simulation of polarization mode dispersion in single mode fibers

To investigate the effects of polarization mode dispersion, we considered a fiber system with parameters as shown in table (3.1). The optical link was made of lossless optical amplifiers with a gain of 20 dB and a noise figure of 6 dB. The link was dispersion uncompensated link with full and ideal GVD compensation before entering the receiver. For the case of the analysis, we focused on an optical link with one span. Two channels, each with a symbol rate of 49 Gbd, were transmitted in the system at different spacings starting with 50 GHz. The digital signal used sinc pulses with Gaussian distributed complex symbols.

We assumed that only inter-modal dispersion was in the play and that intra-modal dispersion between the channels did not exist as was assumed by the authors in [28].

To simulate only the effects of XPM, we set the power of the channel under test to be 30 dB smaller than the interfering channel, such that self-phase modulation was absent of it. The interfering channel had a power of 0 dBm such that XPM was active on the channel under test. Furthermore, we did not include amplified spontaneous emission since our objective was the interaction between mode dispersion and the Kerr effect. Different system parameters like dispersion, attenuation, span length, symbol rate, were varied with the aim of testing the model accuracy evaluated in estimating the variance of XPM.

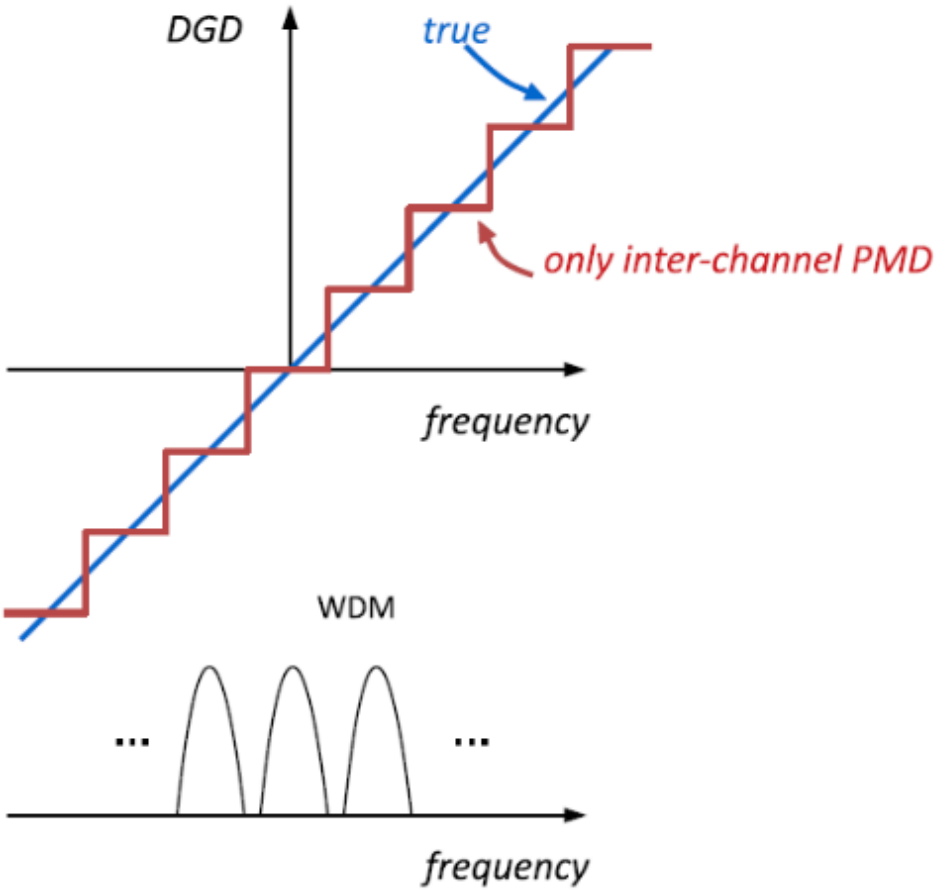

Figure 3.1: The difference between when only inter-channel modal dispersion is considered and when both inter-channel and intra-channel dispersion is considered [31]. The blue plot through the origin is when full PMD is tested.

Table 3.1: Fiber parameters and their properties

Fiber parameters	**Properties**
Fiber length	100 [km]
Dispersion	17 $[\frac{ps}{nm \cdot km}]$
Attenuation	0.2$[\frac{dB}{km}]$
Nonlinear index n_2	2.5e-20 $[\frac{m^2}{W}]$
Nonlinear coefficient γ	1.26 $[\frac{1}{W.km}]$
Fiber lambda	1550 [nm]
Fiber slope	$-[\frac{2\times\text{Fiber Dispersion}}{\text{Fiber Lambda}}]$
Effective area	80 $[\mu m^2]$

To evaluate the accuracy of the model, we performed SSFM simulations. According to the SSFM algorithm, the non-linear Schrödinger equation can be written as:

$$\frac{dA}{dz} = (L + N[A])A \tag{3.16}$$

and thus the fiber is modelled as:

$$A(z + h, t) = e^{hL} e^{hN} A(z, t) \tag{3.17}$$

such that the operator L takes account of the linear effects and the N operator takes account of the nonlinear effects. The optical fiber is divided into several segments of length h where both the linear and nonlinear effects are considered separately until the entire length of the fiber is analysed. The propagation of an optical signal is considered segment by segment and is analysed in two steps. In each step, we applied the linear/nonlinear effects individually as described by [36]. To improve the accuracy of the SSFM model the segment of length h can be re-halved such that the new segment has a length of $h/2$. The idea can be iterated until observing the saturation of the results. An improved version is the symmetrised SSFM where the step is split as:

$$A(z + h, t) = e^{\frac{hL}{2}} e^{hN} e^{\frac{hL}{2}} A(z, t). \tag{3.18}$$

Due to the presence of PMD, the SSFM simulations rely on the wave-plate model as discussed in Chapter 1. We used 4000 wave plates to test the interaction between PMD and the Kerr effects.

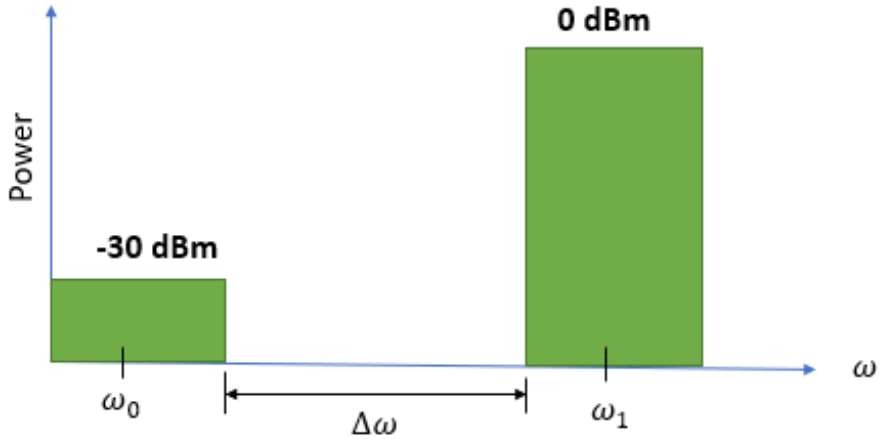

Figure 3.2: Transmitted spectra, showing two channels spaced $\Delta\omega$. The channel under test had 30 dB smaller than the interfering one to suppress SPM.

3.2.1 Numerical results

In order to assess the impact of PMD on the XPM variance, we focused on the relative XPM variance, defined as:

$$\Delta\sigma^2_{\text{xpm}} = \frac{\sigma^2_{\text{xpm}}}{\sigma^2_{\text{xpm,no PMD}}} \tag{3.19}$$

Exploiting the extended Gaussian noise model, we observed a reduction in the relative XPM variance with increasing PMD values and channel spacing as shown in fig. 3.3. For instance, when the channels were spaced at 50 GHz and the PMD value set to 2 ps/sqrt(km), we observed a relative XPM variance of -0.1 dB while if we increased the PMD value to 10 ps/sqrt(km) with the same spacing, we observed an XPM variance of -1.04 dB. When we increased the channel spacing from 50 GHz to 1000 GHz, we observed a relative variance of -1 dB at a PMD of 2 ps/sqrt(km). A further reduction by 0.25 dB was observed when we increased the PMD value to 10 ps/sqrt(km).

The XPM variance continues decreasing with an increasing mode dispersion until a threshold modal dispersion is met after which the XPM variance saturates to its asymptotic value of -1.25 dB [27]. The explanation is that the mode dispersion decorrelates the two channels along the propagation. The process saturates after experiencing full decorrelation.

We validated the XPM formula in (3.13) with SSFM simulations in the presence of only inter-channel PMD. Figure 3.4 shows a good match between the model (markers) and the simulations (solid lines) as high channel spacing. However, a mismatch is observed

for some PMD values when the channel spacing is small. This gap can be attributed to the approximations involved in the derivation of the closed-form expression of the XPM variance. The accuracy can be increased by implementing the Gaussian noise model with numerical integration at the expense of a higher complexity [28]. We did not investigate such an aspect in this work since we focused on ultra-fast expressions that can be used in the real operation of a network. Moreover, the numerical expression require complex algorithm to test them which was out of the scope of this thesis.

Figure 3.5 shows the XPM variance with the increasing polarization mode dispersion when group velocity dispersion is varied. We observe a monotonic behaviour, with the lowest relative variance values at the smallest dispersion. Therefore, we can conclude that the effect of PMD on the XPM variance is less evident at higher dispersion while it is more beneficial at lower dispersion values.

Figure 3.6 shows the results for a wider range of PMD values, hence showing the saturation of the XPM curves. In addition, the figure includes SSFM sanity checks for all the dispersion values,under the assumption of inter-channel PMD. It can be seen that the agreement between the model and the SSFM results is excellent at low dispersion.

When we varied the attenuation from 0.01 dB to 0.2 dB, we recorded a negligible change on the XPM variance as shown in fig. 3.7. We then investigated the effect of symbol rate and we observed that increasing the symbol rate reduces the benefit of PMD on the XPM variance. For instance, at a channel spacing of 100 GHz, 10 Gbd had the highest impact of PMD in reducing the XPM variance compared to the 100 Gbd, both at 2 and 10 ps/sqrt(km) as shown in fig.3.8. The reason is again that at higher symbol rate the decorrelation induced by the GVD walk-off is stronger, thus mitigating the role of PMD.

We then performed SSFM simulation with inter and intra channel PMD, with the aim of investigating the validity of the model derived under the inter-channel PMD assumption. The obtained results is as shown in fig. 3.9 for the same setup as fig. 3.7. We used Gaussian distributed symbols at 49 gigabits per second with the channel spacing 50 GHz. The SSFM simulation conditions set in [37] were respected and the simulations repeated for 1000 different random realization of the wave-plates.

The matching between the model and the SSFM in Fig 3.9 is not good because we included intra-channel PMD in the SSFM while the model only accounts for the inter-channel PMD.

We also tested the model by increasing the number of channels from 2 to 25 as reported. The spacing between the channels were varied and the model tested at different values of the symbol rate. For the first case, we set the channel spacing at 100 GHz and varied the number of channels. We observed that the benefits of PMD on XPM reduces when the number of channels is increased as shown in fig. 3.10. For example, when 25 channels were tested, a normalized XPM variance of -0.8 dB was recorded at a PMD value of 10 ps/sqrt(km), while a variance of -1.18 dB was recorded when 3 channels were tested at the same PMD value. The explanation is that as the number of channels increases, the variance of XPM imposed on the channel of interest increases too as we have to sum all the individual contributions of each channel. Furthermore, we observed

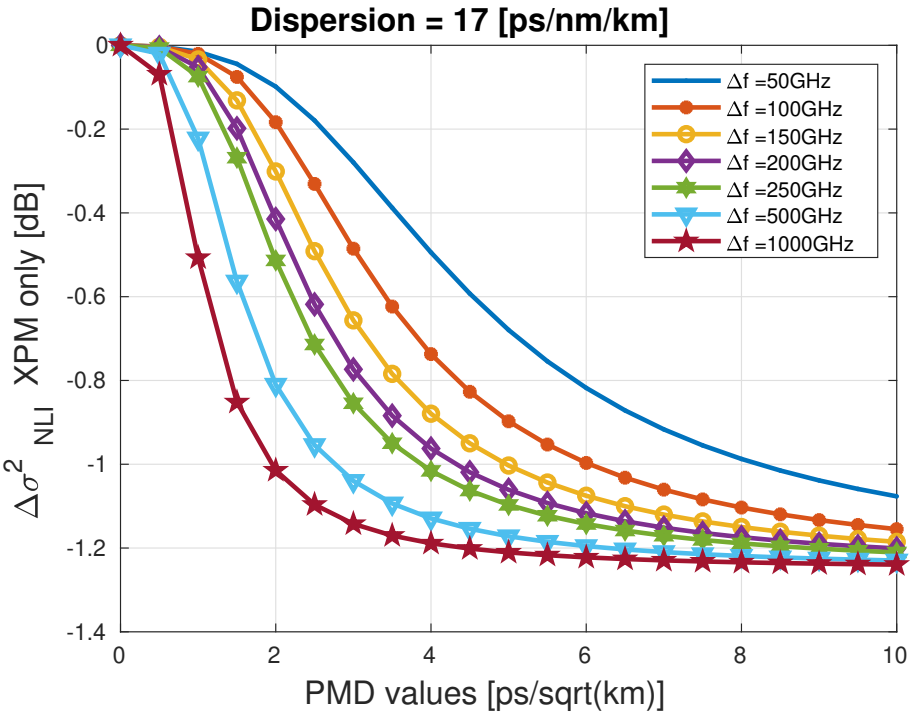

Figure 3.3: The relative variance of XPM with respect to no PMD, reduces with an increase in mode dispersion. The variance is observed to further decrease with an increase in the channel spacing.

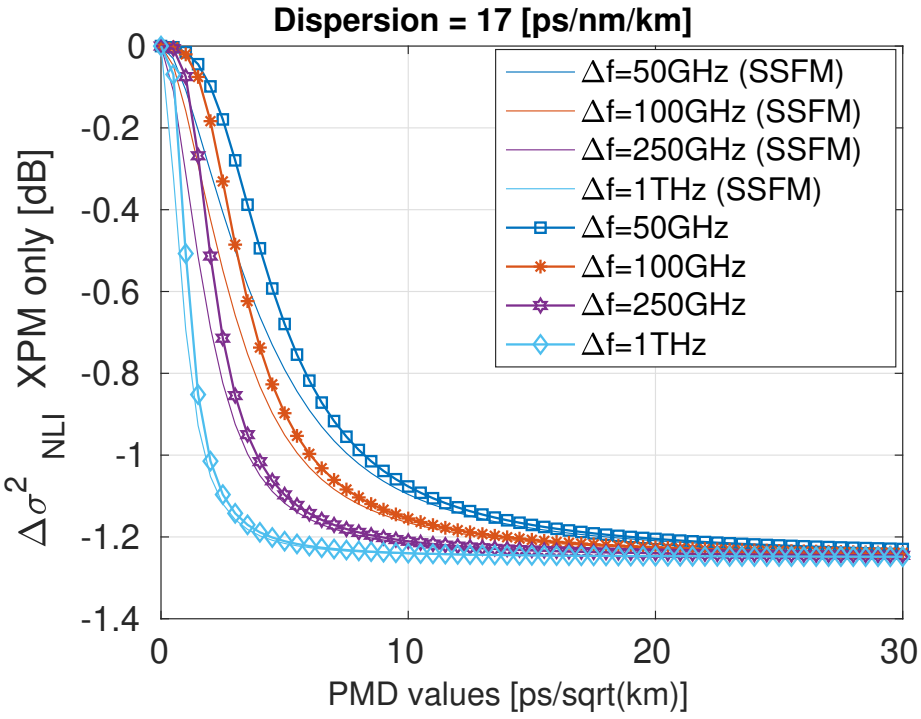

Figure 3.4: The relative XPM variance vs PMD at different channel spacing, by SSFM and the model (3.13)

that even at higher channels count, the larger channel spacing reduced the relative XPM variance as shown in fig. 3.11 for WDM comb of 11 channels.

If we normalize the XPM variance to its value at the channel spacing of 100 GHz, we observed that PMD was beneficial in reducing the relative XPM variance. For instance, the normalized XPM variance reduces more rapidly when the PMD value is increased compared to when there is absence of PMD as shown in fig. 3.12 for 13 channels, and fig. 3.13 for 2, 5 and 9 channels.

3.3 Simulation of mode dispersion in multimode mode fibers

When N in 3.13 is greater than 1, the modal dispersion is referred to as spatial modal dispersion. The key parameter for the strength of modal dispersion is the spatial modal dispersion (SMD), which is related to the μ parameter [28] by:

$$\mu = \frac{SMD}{\sqrt{\frac{4N^2-1}{2N^2}} \times \sqrt{\frac{N}{2}}} \tag{3.20}$$

We simulate the two channels each transmitting 49 Gbd at a spacing of 100 GHz. The modulation format was Gaussian distributed symbols with 65536 symbols. We used the same parameters as in the previous section, by substituting the fiber with a SDM fiber supporting strongly coupled modes. The Manakov coefficient changes from the factor of dual polarization shown in [29] to

$$\kappa = \frac{4}{3}\frac{2N}{2N+1} \tag{3.21}$$

where the coefficient is dependent on the number of modes. We varied the nonlinear coefficient γ such that the the new nonlinear coefficient γ_{new}, was dependent on the number of modes, i.e.

$$\gamma_{new} = \frac{\gamma_{sc}}{N}. \tag{3.22}$$

We also changed the number of modes starting at N=2 up to N=6 and set the other fiber parameters as shown in table (3.1).

3.3.1 Numerical results

When the number of modes is increased, we observe a decrease in the XPM variance and a further decrease with increasing spatial modal dispersion values as shown in fig. 3.14. For example, when N=2 at 0 SMD value, we observe a power normalized XPM variance of -50.2dB, while when the modal dispersion is increased to 12 ps/sqrt(km), we observe a variance of approximate of -52 dB at the same value of N. If N is increased to 6, an XPM variance of -54.5 dB is recorded when the SMD value is 0. A further reduction by almost 3 dB is observed when the modal dispersion value increased to 12 ps/sqrt(km).

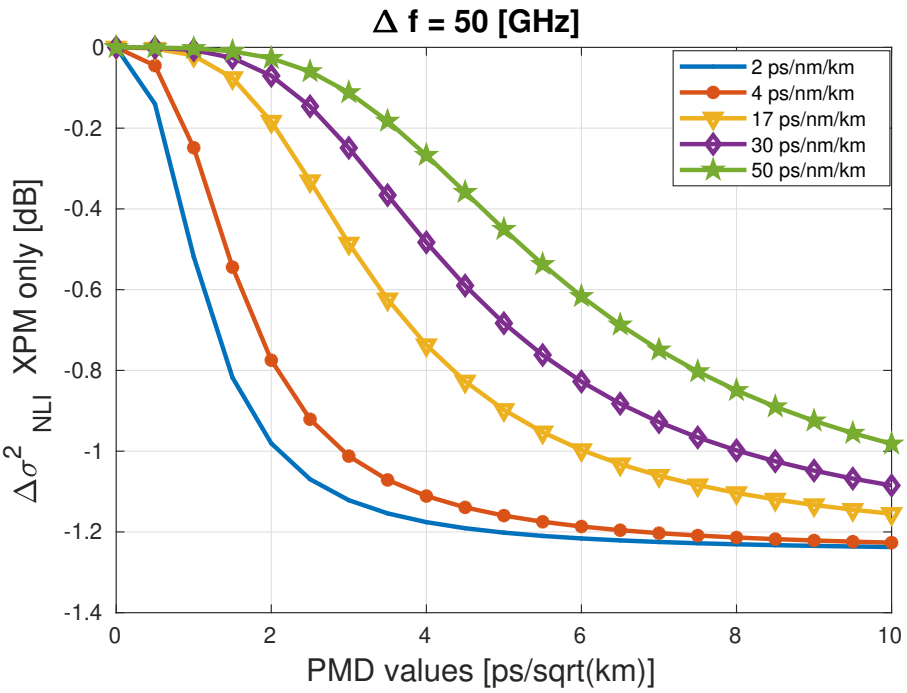

Figure 3.5: The relative variance of XPM versus modal dispersion at different values of the fiber dispersion. Note that the relative variance decreases with a decreasing dispersion value.

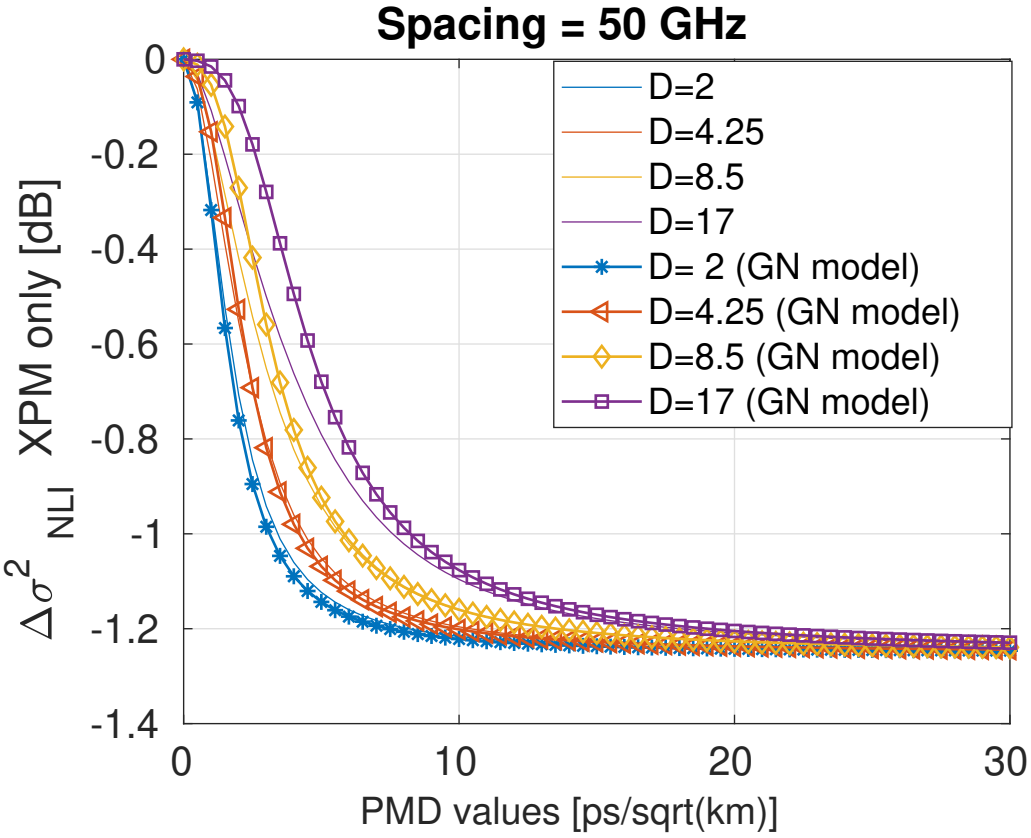

Figure 3.6: GN model versus SSFM simulations for a single-span link at variable fiber-dispersion values.

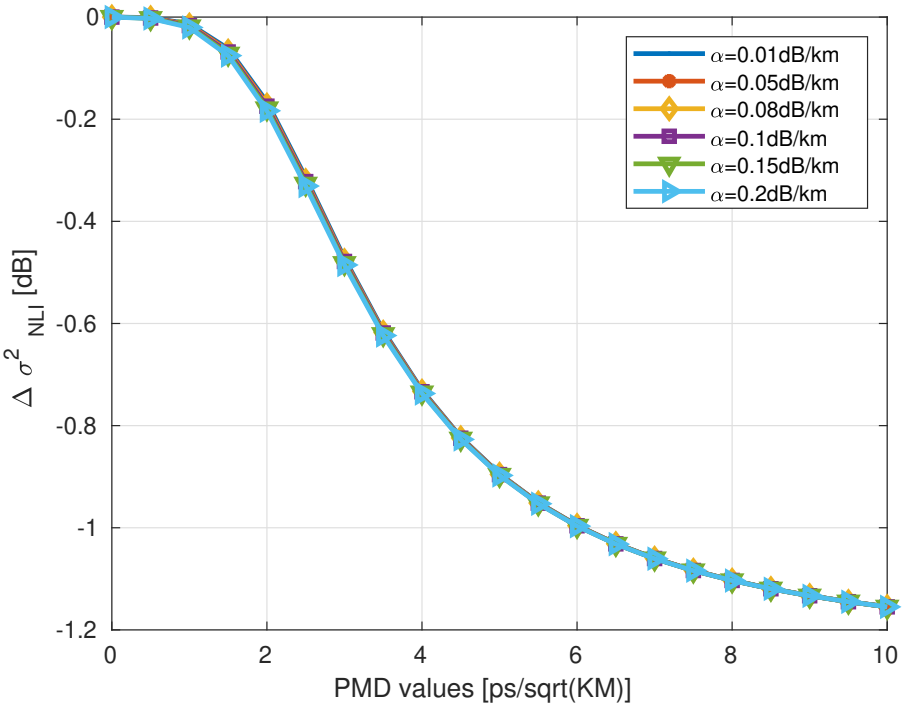

Figure 3.7: The relative variance of XPM, normalized to the value without PMD, vs with PMD at different attenuation values

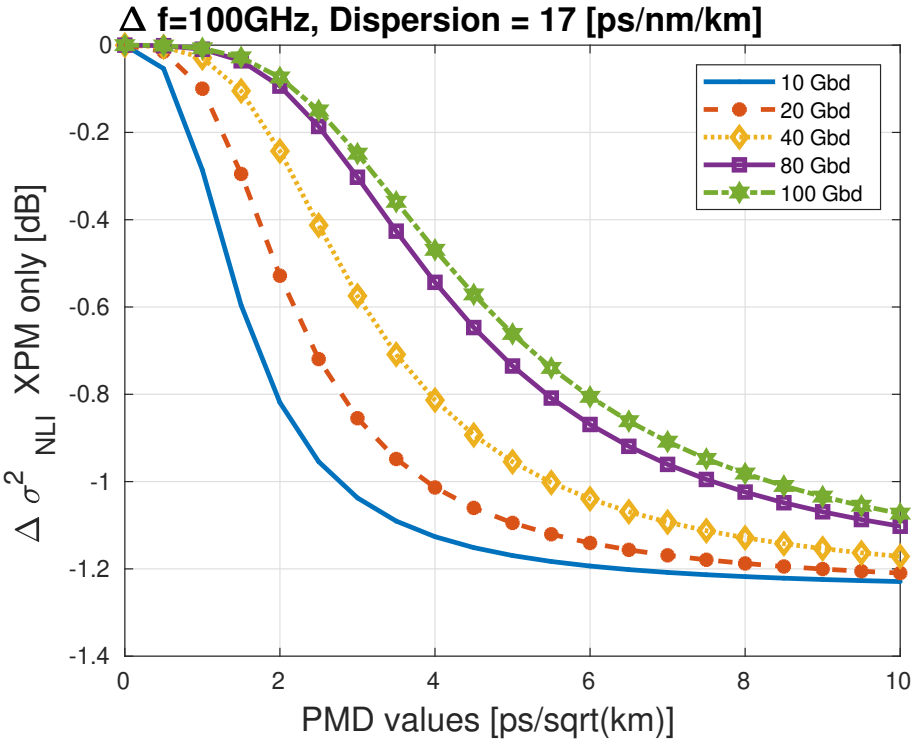

Figure 3.8: The variance of XPM, normalized to the value without PMD, vs PMD at different symbol rates.

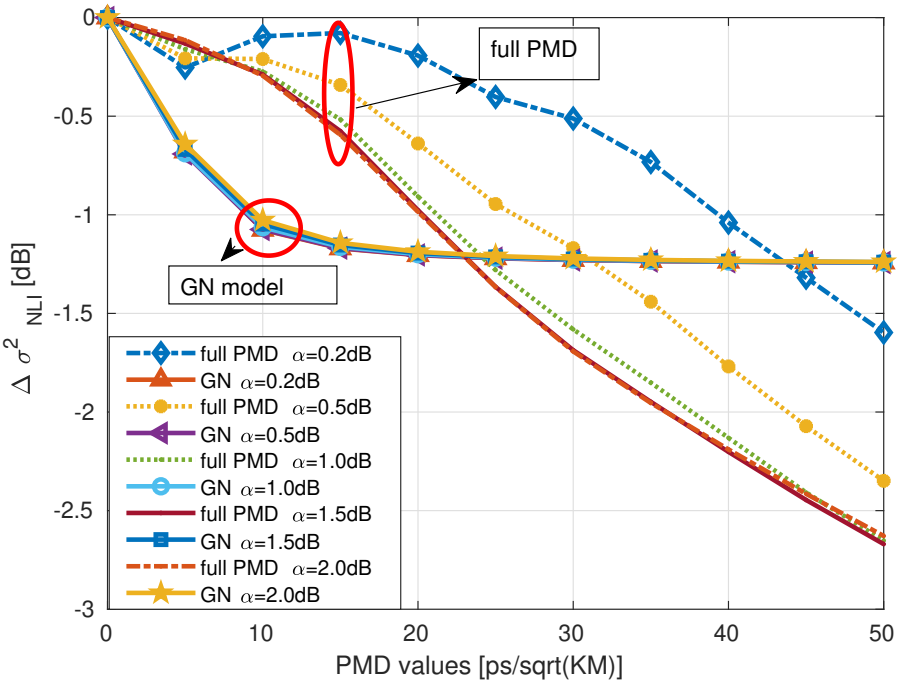

Figure 3.9: XPM variance normalized to the value without PMD vs PMD at variable attenuation. The mismatch the two is related to the presence of intra-channel effects in SSFM, neglected in the GN model.

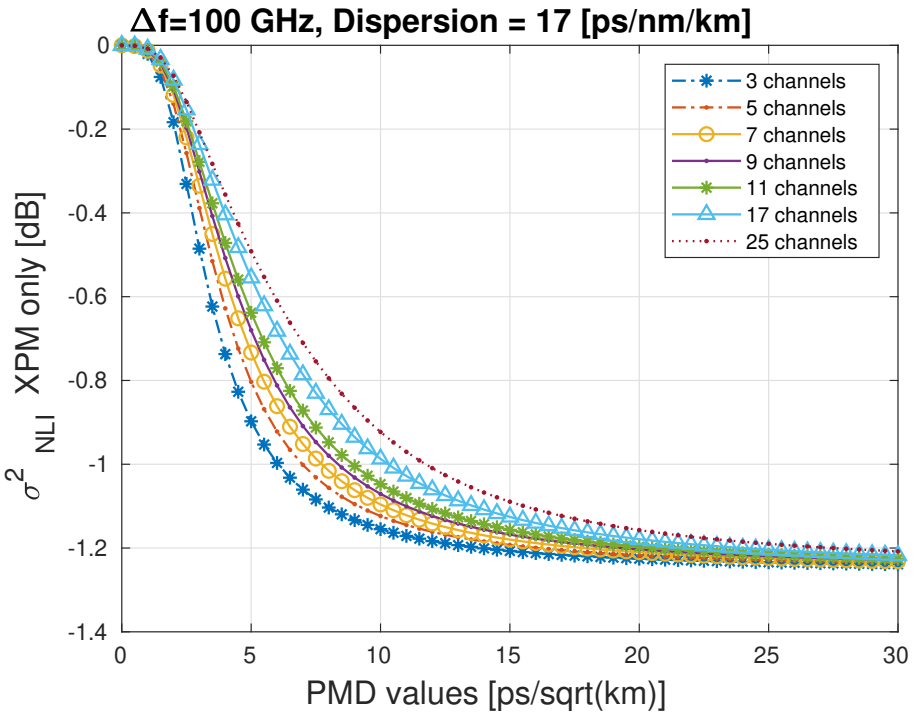

Figure 3.10: The variance of XPM normalized to the value without PMD vs PMD. Different number channels at 49 Gbd are tested on the model.

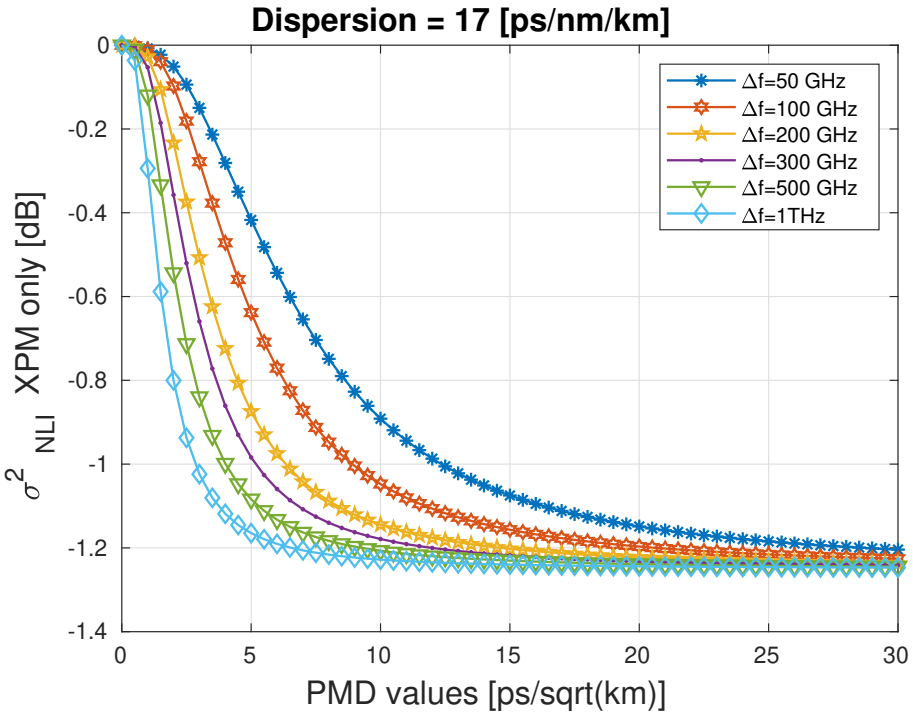

Figure 3.11: The variance of XPM at different channel spacing values when 11 channels are tested on the model.

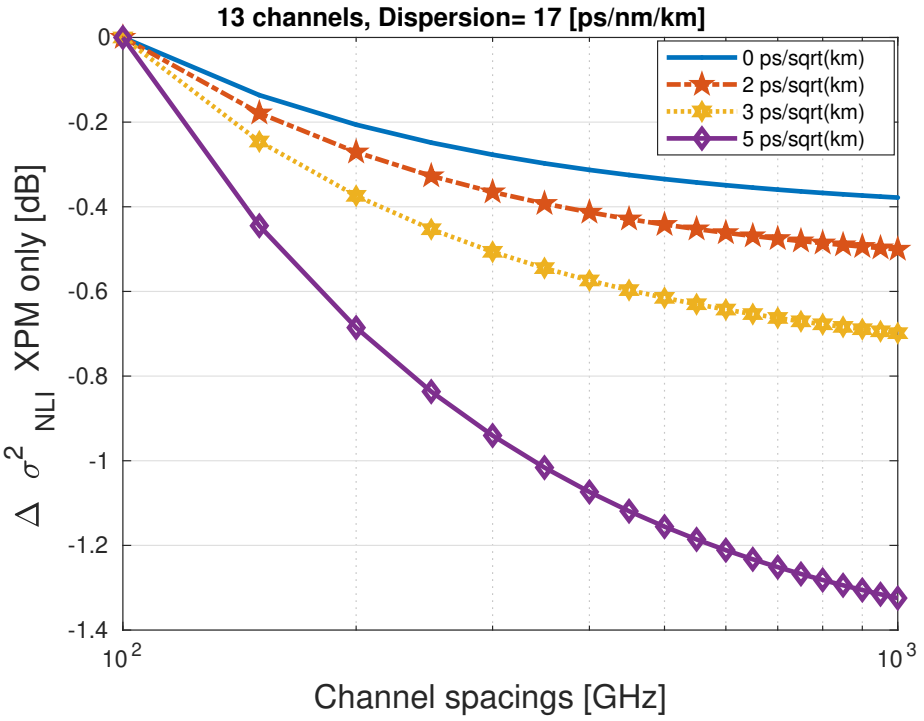

Figure 3.12: The variance of XPM when 13 channels at different spacings and PMD values are tested on the model.

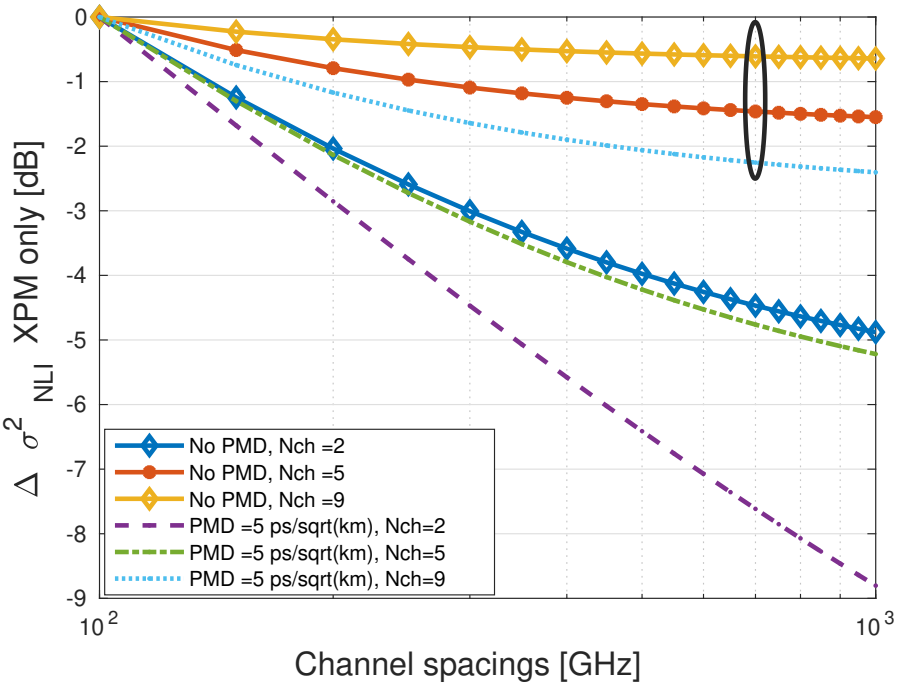

Figure 3.13: The variance of XPM at different number of channels when PMD value is 0 (plots with symbols) and 5ps/sqrt(km). The ellipse shows the difference in variance when 9 channels with or without PMD.

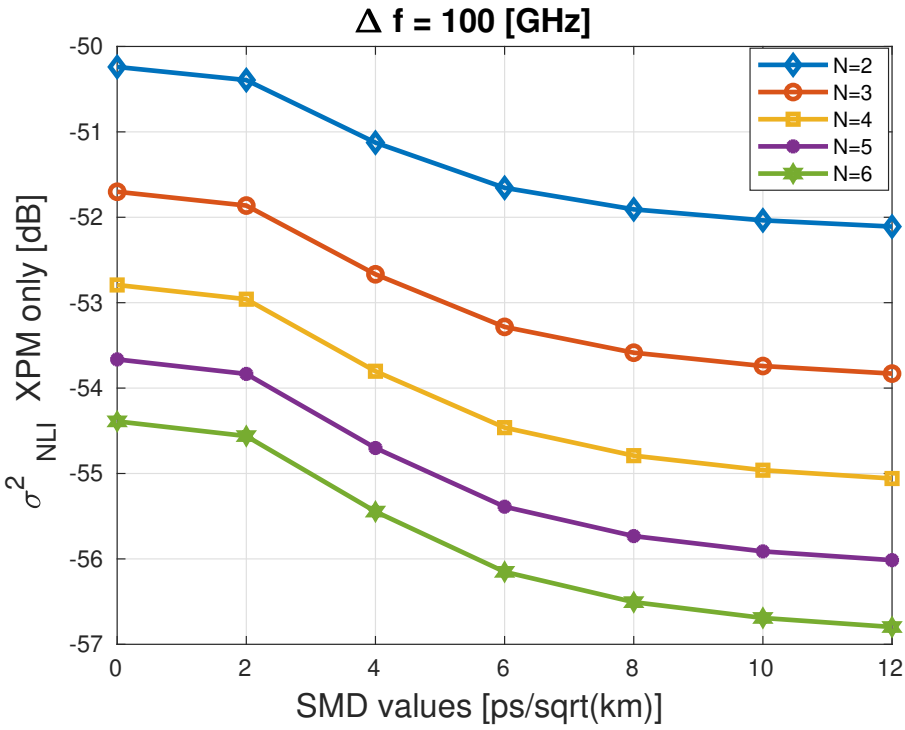

Figure 3.14: The variance of XPM with the mode dispersion when the number of modes is varied.

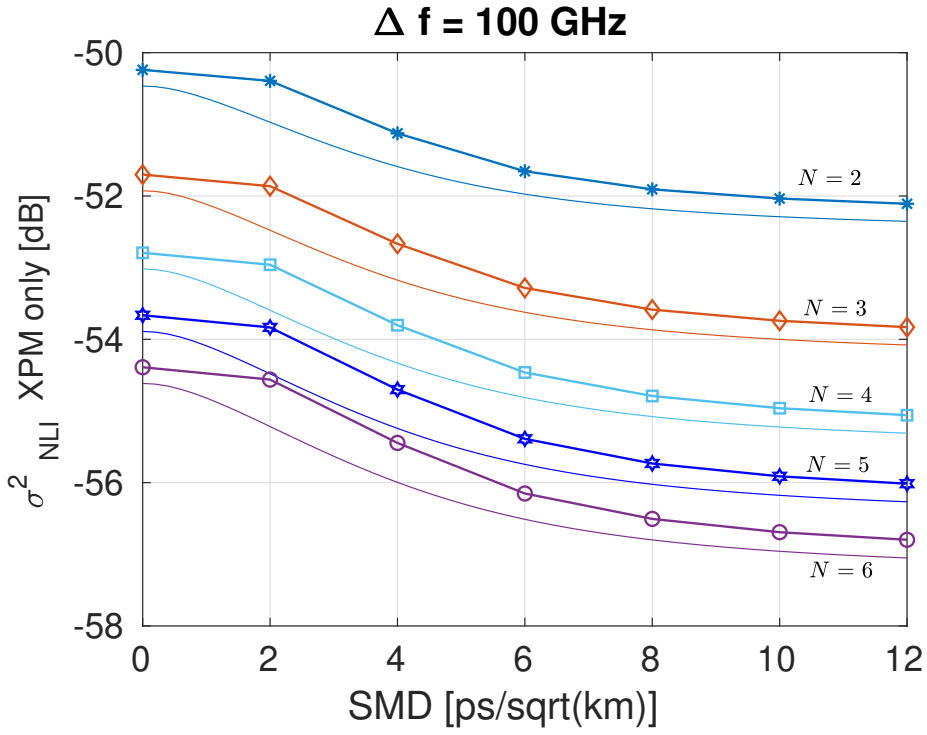

Figure 3.15: XPM variance estimated with the GN model (symbols) and the SSFM (no symbols).

Such result confirms that the variance of XPM reduces with an increasing number of modes because of the new non-linearity coefficient which is dependent on the number of modes given by:

$$\kappa\gamma_{sc}\frac{2N+1}{4N} \tag{3.23}$$

where γ_{sc} is the nonlinear coefficient in the scalar case. The quality of transmission determined by the SNR of each mode can be calculated as

$$SNR = \frac{P}{P_{ASE} + P_{NL}} \tag{3.24}$$

where P_{NL} is given as

$$P_{NL} = 2N\left(\kappa\gamma_{sc}\frac{2N+1}{4N}\right)P_{NL,scalar} \tag{3.25}$$

as shown in [25]. P is the power allocated in each mode and $P_{NL,scalar}$ is equivalent to χP^3 derived in [38]. An optimal SNR exists and is given by

$$SNR_{opt} = \left(\frac{4N}{2N+1}\right)^{\frac{2}{3}} \times \frac{2^{\frac{2}{3}}}{3\left(\sqrt{\chi}\gamma P_{ASE}\right)^{\frac{2}{3}}} \times \left[\sqrt{2N}\kappa(N)\right], \tag{3.26}$$

when we maximise P in (3.24). We can deduce from (3.26) that SNR_{opt} is proportional to $\mathrm{N}^{\frac{1}{3}}$ because of the dependence of κ on N when $N \gg 1$. This shows that we can send several strongly coupled modes along the fiber and take the advantage of mode dispersion reducing the non-linearities impacting on the value of SNR. Figure 3.15 shows a close similarity between the GN model and SSFM simulations for any value of N modes with only inter-channel SMD. As was discussed previously, the discrepancy between the plots results from the approximation errors made in [29].

Figure 3.16 and 3.17 depict the XPM variance in SDM for two different number of modes N. We observe a different strength of the SMD-modified XPM variance by varying N. For instance, at N=6 the XPM variance decreases by 2.7 dB at a symbol rate of 10 Gbd with respect to the no SMD case, while at N=2 the decrease is only 1.6 dB. By increasing the channel spacing to 1000 GHz , we observed almost 1.2 dB difference between N=2 and N=6 at 30 ps/sqrt(km). This confirms our observation that the far away channels have a smaller impact on the XPM variance than in SMF. This observation may be useful in reducing the effort of a possible nonlinear mitigation algorithm when applied to a superchannel made of several channels.

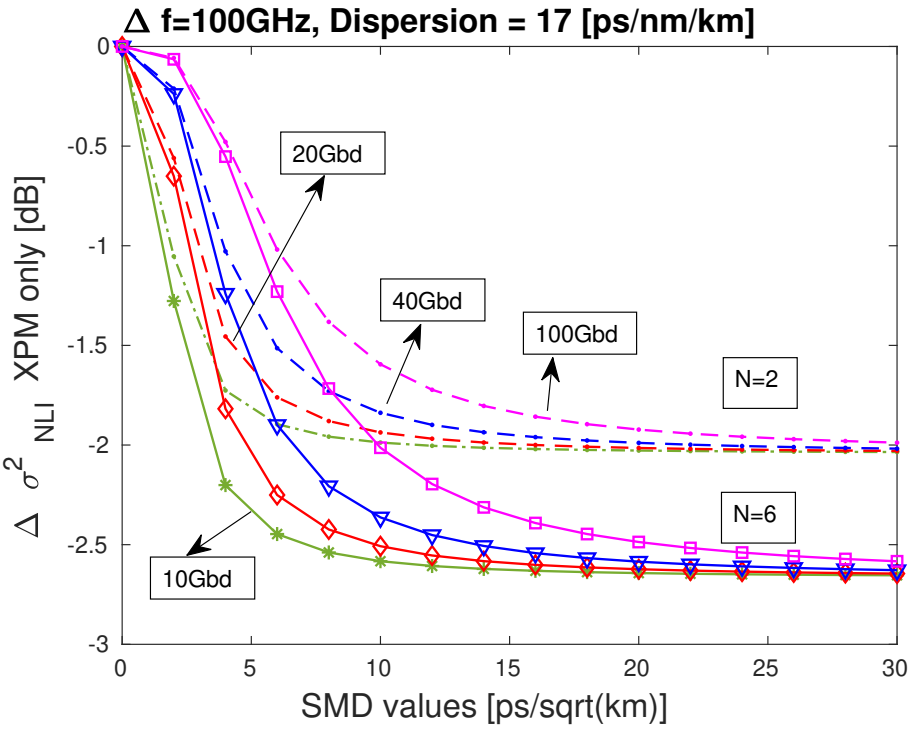

Figure 3.16: Comparing the variance of XPM with mode dispersion when the symbol rate is varied. The dotted plots are when N=2.

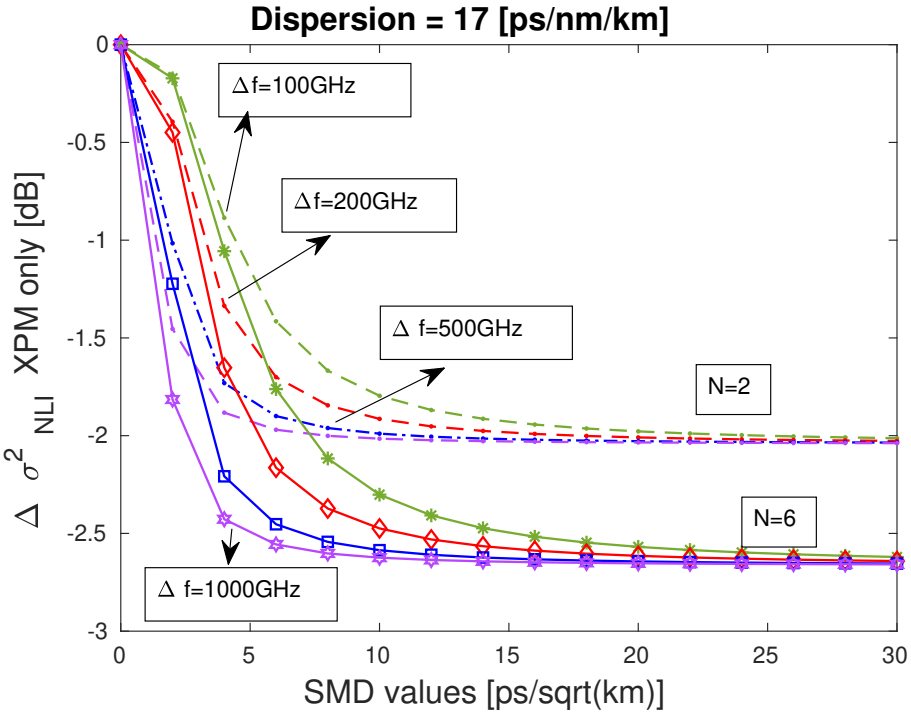

Figure 3.17: Shows the variance of XPM with the mode dispersion when the number of modes and channel spacing are varied. The plots with symbols represents when N=6.

Conclusion

The introduction of new technologies like the internet of things, cloud computing, and more people and devices getting connected to the internet is leading to higher demands for data. The problem is that the capacity of the existing optical network - mostly composed of single-mode fibers-is limited by non-linearities. Researchers are working on new technologies to find a possibility of meeting these data demands and one such technology is space-division multiplexing. Just like single-mode fibers, the capacity of multimode or multi-core fibers is influenced by the nonlinear impairments and therefore the need to find solutions to combat or eradicate these effects.

In this thesis, we discussed the linear impairments in Chapter 1, starting with the impairments experienced in single mode fibers and extended them to multimode fibers. We observed that when spatial multiplexing is considered, it is impossible to omit modal dispersion which can exist in the form of polarization mode dispersion in single mode fiber or as spatial mode dispersion in the multimode case. We discussed the coupling models and the advantages arising from mode coupling.

In chapter 2, we discussed the nonlinear impairments in single mode fibers which occur in the form of self-phase modulation, four wave mixing, cross phase modulation. We extended the impairments to the multimode domain discussing both inter and intra-group interference and we observed that in the presence of mode dispersion, the effects of nonlinear interference can be reduced.

in Chapter 3 we focused on a simplified model to describe the interaction of the Kerr effect with the mode dispersion in a fast, yet approximated, way.

We simulated the Gaussian noise model extended to accommodate modal dispersion in Chapter 3. Thanks to the short computational time of the extended model, we tested different optical system at variable parameters including dispersion, channel spacing, attenuation. We observed that modal dispersion is beneficial in combating non-linearities, especially cross-phase modulation which is the dominant impairment at higher data rates when implemented with other system parameters. We double-checked our results using the SSFM simulations. Furthermore, we also observed that transmitting several modes on a multimode fiber reduces the impact of the nonlinear impairments on the signal-to-noise ratio and therefore we can take the advantage of modal dispersion to meet the demands at a better quality of transmission.

Future work is open to exploring the effects of intra-channel modal dispersion on

the non-linearities and modelling the effects of self-phase modulation in the presence of dispersion.

Bibliography

Bibliography

[1] W. Pratt, *Laser Communication Systems*, Wiley, New York, 1969.

[2] C. Kao and G. A. Hockham, 'Dielectric fiber surface waveguides for optical frequencies ', Proc. IEE, 113(7), pp. 1151–1158, 1966.

[3] A. Chralyvy, "The Coming Capacity Crunch", Bell Labs, Alcatel-Lucent, USA-ECOC 2009, 20-24 September, 2009, Vienna, Austria.

[4] *Network traffic insights in the time of COVID-19: April 9update*, https://www.nokia.com/blog/network-traffic-insights-time-covid-19-april-9-update

[5] *Cisco Visual Networking Index: Forecast and Trends, 2017-2022*, short-url.at/gijrB

[6] P. Mitra and J. Stark 'Nonlinear limits to the information capacity of optical fibre communications 'Letters to Nature, Vol 411, June 2001

[7] R. Essiambre 'Fiber Capacity Limits: Information Theory meets Optical Communication and Fiber Physics 'Bell Labs, Alcatel-Lucent, New Jersey, 07733, USA

[8] C.Shannon 'A Mathematical Theory of Communication 'The Bell System Technical Journal, Vol. 27, July, October, 1948.

[9] T. Morioka 'High-Capacity Transmission Using High-Density Multicore Fiber,'OFC 2017.

[10] E. Pincemin 'Towards Multi-Band WDM Systems with Hundreds of Terabit/s Transported on one Single-Mode Fiber,'2021 IEEE Summer Topical Meeting Series,July 2021, Paper ME1.2/Optical Networks Session

[11] J. Fischer, M. Sena, et al, 'Perspectives of optical transmitters for Multi-band Transmission Systems '2021 IEEE Summer Topical Meeting Series, July 2021

[12] K.Po and J. Kahn 'Mode Coupling and its Impact on Spatially Multiplexed Systems ', Chapter 11

[13] D. Marcuse, Theory of Dielectric Optical Waveguide, second ed., Academic Press, 1991.

[14] G. Agrawal, "Fiber Optic Communication Systems", A. John Willey and Sons Publications, 4th Edition, 2010

[15] F. Curti,B.Diano, Q.Mao, F.Matera, and G. Someda ,"Concatenation of Polarisation Dispersion in Single Mode Fibers", Electron Lett., vol 25. pp 290-292. 1989

[16] J.Elbers, C.Lingener, M.Duser,and E.Voges ,"Polarisation Mode Dispersion in Single Mode Fibers", Electron Lett., vol 33, No 22, pp 1894-1895. 1997

[17] R. Ryf, S. Randel, A. Gnauck, et al, "Mode-division multiplexing over 96 km of few-mode fiber using coherent 6 × 6 MIMO", J. Lightw. Technol., Vol 30, pp 521–531,2012.

[18] S. Arik, D. Askarov, J.Kahn, "Effect of mode coupling on signal processing complexity in mode-division multiplexing", J. Lightw. Technol., Vol 31, pp 423–431,2013.

[19] K. Ho, J.M. Kahn, "Frequency diversity in mode-division multiplexing systems", J. Light. Technol., Vol 29, pp. 3719–3726, 2011.

[20] R. Ryf ., "1705-km transmission over coupled-core fibre supporting 6 spatial modes," presented at the Eur. Conf. Optical Communication, Cannes, France, 2014, Paper PD.3.2

[21] C. Antonelli, A. Mecozzi, M. Shtaif, and P. J. Winzer, "Random coupling between groups of degenerate fiber modes in mode multiplexed transmission," Opt. Exp., vol. 21, pp. 9484–9490, 2013.

[22] R. W. Boyd, "Nonlinear Optics" (Academic Press, San Diego, CA, 1992).

[23] G. Agrawal, "Nonlinear Fiber Optics" (Academic Press, San Diego, CA, 2001).

[24] A Vannucci, P Serena, A Bononi, "The RP method: A new tool for the iterative solution of the nonlinear Schrödinger equation" J. Lightw. Technol., Vol. 20, no. 7, 2002.

[25] C. Antonelli, A. Mecozzi,and M. Shtaif,"Modelling of Nonlinear Propagation in Space-Division Multiplexed Fiber-Optic Transmission", J. Lightw. Technol., Vol.34, No.1, 2016

[26] A.Mecozzi, C. Antonelli,and M.Shtaif,"Nonlinear Equations of Propagation in Multi-Mode Fibers with Random Mode Coupling" ECOC 2017, paper We.3.D.3

[27] C. Antonelli, O. Golani, M. Shtaif, and A. Mecozzi, "Nonlinear interference noise in space-division multiplexed transmission through optical fibers" Optics Express, Vol. 25, No. 12 ,pp.13055-13075, 2017

[28] P. Serena, C.Lasagni, A. Bononi , C. Antonelli, and A. Mecozzi, "A Model of the Nonlinear Interference in Space-Division Multiplexed Systems with Arbitrary Modal Dispersion"- ECOC 2021, paper Tu2DE.

[29] P. Poggiolini, G. Bosco, A. Carena, V. Curri, Y. Jiang, and F. Forghieri, "The GN-Model of Fiber Non-Linear Propagation and its Applications," J. Lightw. Technol., vol. 32, no. 4, pp. 694–721, 2014.

[30] R. Dar, M. Feder, A. Mecozzi, and M. Shtaif, "Pulse collision picture of inter-channel nonlinear interference noise in fiber-optic communications," J. Lightw. Technol, vol. 34, no. 2, pp. 593–607, 2016

[31] P. Serena, C.Lasagni, A. Bononi , "GN model Extended to Modal Dispersion"- PRIN Meeting, Universita di Parma, Feb 2021

[32] P. Poggiolini, G. Bosco, A. Carena, V. Curri, Y. Jiang, and F. Forghieri, "A Detailed Analytical Derivation of the GN Model of Non-Linear Interference in Coherent Optical Transmission Systems," *arXiv:1209.0394*, 2012

[33] P. Serena, C.Lasagni, A. Bononi "The Enhanced Gaussian Noise Model Extended to Polarization-Dependent Loss" J. Lightw. Technol., vol. 38, no. 20, pp. 5685–5693, 2020.

[34] G. Rademacher and K. Petermann, "Nonlinear Gaussian Noise Model for Multimode Fibers with Space-Division Multiplexing," J. Lightw. Technol, vol. 34, no. 9, pp. 2280–2287, 2016.

[35] A. D. Ellis, N. Mac Suibhne, F. C. G. Gunning, and S. Sygletos, "Expressions for the nonlinear transmission performance of multi-mode optical fiber," Opt. Express, vol. 21, no. 19, p. 22834-22846, 2013.

[36] 0. V. Sinkin, R. Holzlohner, J. Zweck, and C. R. Menyuk, "Optimization of the split-step Fourier method in modeling optical-fiber communications systems," J. Lightw. Technol, vol. 21, pp. 61-68,2003.

[37] P. Serena, C. Lasagni, A. Bononi ,"On Numerical Simulations of Ultra-Wideband Long-Haul Optical Communication Systems" J. Lightw. Technol, vol. 38, no. 5, pp. 1019– 1030, 2020.

[38] R. Dar, M. Feder, A. Mecozzi, and M. Shtaif, "Properties of nonlinear noise in long, dispersion-uncompensated fiber links," Opt. Exp., vol. 21, pp. 25685–25699, 2013.

Acknowledgements

"Everything that has a beginning comes to an end," said Marcus Quintilianus, a medieval Roman educator. The journey that started in September 2018 is coming to an end, but before that, I have to appreciate all the people that made it happen in this section. First of all, I would like to thank my thesis advisor, Prof. Paolo Serena. Firstly, for introducing me to the concept of optical communications from the basic to the advanced level. Secondly, I want to thank him for always being available to advise me and answer my concerns promptly during the thesis period, and helping me understand advanced concepts in a very easy manner. As I start a new journey in the field of optical networks, the teachings and research experience learned from him will always be invaluable.

Secondly, I very special thanks to my co-advisor Ms. Chiara Lasagni for always being available and providing solutions to my concerns. I want to appreciate her for teaching me several ways and tricks to run scripts and simulations.

My special gratitude goes to my family in different continents especially my mum, my brother Meshack and his wife Ivy for facilitating my arrival and stay in Italy. My sister Angela and Wendy for your extensive support during my masters' studies. Amos and Ullah for your support every summer holiday in Denmark, and all my other family members not mentioned, all your efforts were highly appreciated.

Finally, I want to thank my friends and colleagues I met during my study in Italy, my special friends Matteo, Abdullah, and many others not mentioned. I can't finish without also appreciating the entire faculty of Communication Engineering for sharing their knowledge and instilling me with the useful concepts in the ICT.